Master's thesis

NTNU
Norwegian University of Science and Technology
Faculty of Information Technology and Electrical Engineering
Department of Electronic Systems

Karoline Kjelsaas

# Detection of Air Emboli in the Brain of Neonates by Ultrasound Doppler

Master's thesis in Electronic Systems Design and Innovation
Supervisor: Ilangko Balasingham / Hans Torp
August 2020

NTNU
Norwegian University of Science and Technology

Karoline Kjelsaas

# Detection of Air Emboli in the Brain of Neonates by Ultrasound Doppler

Master's thesis in Electronic Systems Design and Innovation
Supervisor: Ilangko Balasingham / Hans Torp
August 2020

Norwegian University of Science and Technology
Faculty of Information Technology and Electrical Engineering
Department of Electronic Systems

NTNU
Norwegian University of
Science and Technology

# Abstract

When infants are born with a heart defect, catheter intervention or heart surgery may fix the issue. Such interventions can cause air bubbles, or emboli, to flow into the blood stream. The exact reason for this is mostly unknown, but the consequences include clogged arteries and other major problems for the patient. A method of detecting when, where and how many bubbles enter the blood stream is important to get an insight of which procedures should and should not be performed. By looking at the ultrasound Doppler image of the cerebral blood flow using the newly developed NeoDoppler system with the accompanying EarlyBird software, the higher intensity echo signals of air bubbles can be recognised among the surrounding blood signal.

Today, the bubbles are counted by manually searching through the ultrasound image of the signal. This is time consuming as it has to be done multiple times to be sure all bubble signals have been detected, and is sometimes done by multiple people to see if they reach the same conclusion. In this project, the aim is to develop an automatic detection algorithm to increase the efficiency and accuracy of the bubble detection compared to manually going through each recording. The algorithm automatically goes through each depth and counts signals with an intensity above a threshold. To be detected as bubbles, the signal length is compared to an expected bubble length found by the Doppler shift. The algorithm also checks that the high intensity signal is not an artifact caused by medical instruments, and estimates the background signal by median filtering. By trial and error, the threshold giving most correct detections with as few false positives as possible for all 16 recordings in the training set was 9 dB above the background signal. A low pass filter with a cutoff frequency of 20 Hz proved to discard most of the unwanted false detections in recordings with no bubbles. The algorithm has a run time of roughly 30 seconds for a 30 minute recording. With the mentioned settings, the training set had in total 59 correct, 10 false positive and 39 missed detections compared to the manual counting.

The test set used for final evaluation of the algorithm consisted of 405 recordings from 16 patients during catheter intervention and 2 patients with recordings pre, during and post heart surgery. The test set had 1623 detections where 1337 were false positives, mostly due to cyclic variations with the heart frequency. In a smaller data set, 84.6% of false positives were due to cyclic variations. Other reasons are movement of the ultrasound probe, double detections and pulsations of the artery wall. There were not many examples of this in the training set, which is why the algorithm does not compensate for these types of false positives. To improve the rate of correct detections, artifacts of these types should be avoided by adding functions taking each type of false detection into consideration. This could also make it possible to lower the threshold, increasing the number of correct and reducing the number of missed detections.

# Sammendrag

Når spedbarn er født med en form for hjertefeil kan kateterintervensjon eller hjertekirurgi hjelpe. Dette kan føre til at luftbobler, eller embolier, kommer inn i blodstrømmen. Årsaken er for det meste ukjent, men konsekvensene kan være tette arterier og andre alvorlige komplikasjoner hos pasienten. En metode for å detektere når, hvor og hvor mange bobler som kommer inn i blodstrømmen er viktig for å få et innblikk i hvilke metoder som bør brukes eller unngås. Ved å se på ultralyd Doppler-bildet av den cerebrale blodstrømmen, målt med det nylig utviklede NeoDoppler-systemet og det tilhørende EarlyBird-programmet, kan ekkosignalene fra bobler med høyere intensitet gjenkjennes blant blodsignalet.

I dag telles boblene ved å søke gjennom ultralydbildet av signalet manuelt. Dette er tidkrevende siden det må gjøres flere ganger for å være sikker på at alle boblesignaler har blitt telt, og det må noen ganger gjennomføres av flere personer for å se om de kommer fram til det samme. Dette prosjektet hadde som mål å utvikle en automatisk deteksjons-algoritme for å detektere bobler mer effektivt og nøyaktig enn manuelt å gå gjennom alle dybder av hvert opptak i ultralydbildet. Algoritmen går automatisk gjennom hver dybde og teller signaler med intensitet over en viss terskel. For å bli detektert som en boble, blir lengden av signalet sammenliknet med en forventet boblelengde funnet ved Dopplerskiftet. I algoritmen sjekkes det også at signalet ikke kommer av medisinske instrumenter, og et bakgrunnssignal estimeres ved medianfiltrering. Ved å prøve og feile ble det funnet at terskelverdien som ga flest korrekte deteksjoner med så få falske positive som mulig for alle 16 opptak i treningssettet var 9 dB over bakgrunnssignalet. Et lavpassfilter med cutoff-frekvens på 20 Hz fjernet også de fleste falske deteksjonene i opptak uten bobler. Algoritmen har en kjøretid på omtrent 30 sekunder for et 30 minutter langt opptak. Med de nevnte innstillingene ga treningssettet 59 riktige, 10 falske positive og 39 tapte deteksjoner sammenliknet med de manuelt telte boblene.

Testsettet som ble brukt for endelig evaluering av algoritmen besto av 405 opptak fra 16 pasienter under kateterintervensjon og 2 pasienter med opptak før, under og etter hjerte-kirurgi. Testsettet hadde 1623 deteksjoner der 1337 av dem var falske positive, for det meste grunnet sykliske variasjoner med hjertefrekvensen. I et mindre datasett var 84.6% av de falske positive på grunn av sykliske variasjoner. Andre grunner er bevegelse av ultralydproben, doble deteksjoner og pulsasjoner av blodåreveggen. Det var ikke mange eksempler på dette i treningssettet, som er grunnen til at algoritmen ikke kompenserer for disse typene falske positive. For å få flere riktige deteksjoner må artefakter av disse typene gjenkjennes ved å lage funksjoner som tar seg av hver sin type falsk deteksjon i algoritmen. Dette kan også gjøre det mulig å senke terskelen så flere bobler detekteres riktig uten for mange falske.

# Preface

This thesis is written as part of the five year master's program Electronic Systems Design and Innovation at the Norwegian University of Science and Technology, NTNU, at the Department of Electronic Systems. The chosen major is Signal Processing and Communications with a minor in ICT in Health. It was written over the spring semester of 2020 in collaboration with the Department of Circulation and Medical Imaging.

I wish to thank my supervisor Hans Torp for invaluable guidance and feedback throughout the semester, and for being available whenever I needed help, also during the Covid-19 lock down. I would also like to thank Martin Leth-Olsen and Siri Ann Nyrnes at St. Olavs Hospital for their contributions to data collection and for valuable inputs and perspectives throughout the project.

Fetsund, August 2020
Karoline Kjelsaas

# Table of Contents

# List of Tables

# List of Figures

# Abbreviations

| | | |
|---|---|---|
| PMD | = | Power M-mode Doppler |
| TCD | = | Transcranial Doppler |
| CW | = | Continuous Wave |
| PW | = | Pulsed Wave |
| dB | = | Decibel |
| IQ-signal | = | In-phase and Quadrature signal |
| PRF | = | Pulse Repetition Frequency |
| LPF | = | Low Pass Filter |
| FIR | = | Finite Impulse Response |
| IIR | = | Infinite Impulse Response |
| EBR | = | maximum Emboli amplitude to Background amplitude Ratio |

Chapter 1

# Introduction

## 1.1 Background and Motivation

Emboli, or air bubbles, in blood vessels can cause major problems to patients. When a patient, an infant in the case of this project, goes through a cardiac surgery with use of a heart-lung machine, the heart needs to be completely emptied of blood. After the surgery, the heart is filled with blood once more, which can lead to air bubbles entering the arteries, travelling to organs in the body [O'Brien et al. [1997]]. Large air bubbles can block the path like blood clots, leading to oxygen deficiency in the given organ, most relevant to this project, in the brain. There are different methods of refilling the heart after heart surgery, but their impact on the appearance of air bubbles is unknown. Bubbles also appear in the arteries during catheter interventions to fix heart defects. In these cases a heart-lung machine is not used and the reason for air bubbles is not understood.

During surgery, or in clinical situations, with today's technology it is difficult to know how many bubbles are in the blood stream, and how big they are. In experimental research, however, the bubbles are usually counted manually by looking at the m-mode or ultrasound Doppler image of a blood vessel, counting any points with a higher intensity in one or multiple depths. Not only is counting bubbles manually time consuming, the results may vary depending on who is counting and what criteria they use to separate bubbles from the surrounding blood signal. The counting therefore needs to be done multiple times and by different people who know the criteria in order to be credible. This is not something that can realistically be done in real time, which is why an automatic detection algorithm would be an advantage.

An algorithm that automatically detects and counts bubbles using an m-mode image of the blood vessel, either in one or multiple depths at the same time, would save a lot of time and might make it possible to get an overview of bubbles in the bloodstream for clinical use. Such an algorithm will objectively count the same way every single time using the same sets of criteria. This will save a lot of time for experimental studies, and might also make it possible for doctors to see how many bubbles are present in real time

and therefore what methods should be used or avoided considering the appearance of air bubbles.

### 1.1.1 Literature Review

Counting emboli from ultrasound imaging has been done in a few different ways. The research report *Improved Detection of Microbubble Signals Using Power M-Mode Doppler* [Saqqur et al. [2004]] describes criteria for counting embolic signals. For the Power M-mode Doppler (PMD) Transcranial Doppler (TCD), the report gives the following criteria:

1. ""Embolic signature" visible at least 3 dB higher than the highest spontaneous PMD display of background blood flow signal."

2. ""Embolic signature" reflects motion in one direction at a minimum spatial extent of 7.5 mm and a minimum temporal extent of 30 ms. An MCA embolic signature is required to move toward the probe, with a positively sloped track. An ACA embolic signature moves away from the probe, with a negatively sloped track."

3. "The "embolic signature" must traverse a specific depth determined by the highest intensity of the insonated artery in order to avoid repeated counting of the same embolus. For this study we chose the depth defined by the optimal spectrogram waveform."

According to the study, any signal with an intensity above the threshold (at least 3 dB higher than the highest spontaneous power m-mode (PMD) display of background blood flow signal) should thus be registered as a bubble. If there are too many bubbles close together, the number of bubbles will be set to a seamingly random number of 50. The recordings used in this report where from stroke and transient ischaemic attack (TIA) patients, and bubbles were counted using the mentioned criteria. In the detection, the power of the intensity signal in dB was used and compared to a threshold to determine emboli from blood signals.

In the report *Consensus on Microembolus Detection by TCD* [Ringelstein et al. [1998]], TCD ultrasound is used to detect microembolic material within the intracranial cerebral arteries. The goal in this study was to see if microembolus detection in symptomatic patients can recognise individuals at high risk of recurrent stroke. Backscatter from the ultrasound signal of flowing blood is usually lower than that of solid emboli, which can be used for the detection. They used the multigated technique, meaning sampling from several depths to reveal the movement of the embolus and check for artifacts that affect all channels simultaneously.

Another report on this topic is *Power M-Mode Doppler (PMD) for Observing Cerebral Blood Flow and Tracking Emboli* [Moehring et al. [2002]]. Here, transcranial Doppler studies where done while calculating a power m-mode Doppler image. In this case, the user chooses the threshold and sets it for further analysis instead of calculating it based on the In-phase Quadrature signal (IQ-signal). Any power detected below the chosen threshold is assigned no color, meaning black, while anything above is given color depending on its intensity.

A situation with a similar set of patients to the one in this project is described in the article *Cerebral Emboli during Cardiac Surgery in Children* [O'Brien et al. [1997]]. 25 children with congenital cardiac defects went through repairing cardiac surgery while measuring the blood flow with carotid artery Doppler. This was used to observe embolic signals after the fact and connect them to events during the surgery.

## 1.2 Aims of Study

The aim of this project is to develop an algorithm for automatic detection of air bubbles passing through the ultrasound beam. This could be used to learn what procedures should be done during heart surgery or catheter interventions, in this case of infants born with some form of heart defect, to avoid bubbles getting into the blood stream. This algorithm should, given the best threshold, mark all bubbles in an m-mode Doppler image. The more specific goals of the project are therefore:

- To find the best possible threshold to detect bubbles and compare it to the thresholds found in the literature review.
- To detect clouds, or curtains, of bubbles when multiple embolic signals are close together, and find a limit of the bubble length to separate them from singular bubbles.
- To identify artifacts, or signals with a higher intensity from medical instruments or noise, and not count them as bubbles.
- To estimate the number of bubbles passing through the ultrasound beam and the relative size of each bubble.

## 1.3 Outline of the Report

This report is divided into six main chapters, beginning with the introduction, background and motivation and previous work in the field of embolic detection. Further, all background theory is presented to form the basis of the rest of the thesis. Chapter 3 includes the methods to obtain the recordings used in the analysis and the hardware and software systems. It also describes the algorithm developed in this project in detail. All results of the detection and how well the algorithm worked on both the training set and test set will be presented in chapter 4 before discussing it in chapter 5. Finally, before the references and appendix with the complete algorithm, chapter 6 will consider any conclusions that can be made from this project as well as possible future work and improvements.

Chapter 2

# Theory

In this chapter, the theory relevant to the project will be presented, starting with issues emboli can cause to the patient. Following this, the acoustic effects regarding bubbles and blood will be discussed before presenting the ultrasound technology and signal processing used.

## 2.1 Issues Caused by Emboli

Emboli, in this case air bubbles, in blood vessels can cause major problems for the patient. If large enough, the bubbles can clog the artery, leading to blood clots that can prevent oxygen from reaching the brain or other parts of the body. This in turn can cause severe injuries.

Depending on where in the body the bubbles occur, important organs such as the brain, heart, and lungs can get a reduced blood supply causing the organ to lose all or some of its function. This can result in different conditions, one of the most serious being stroke from a blocked blood supply to the brain [NHS [2020]].

There are different reasons why emboli can occur in blood vessels, but with regards to bubbles appearing during heart surgeries, it is commonly due to systemic venous return, meaning when the blood returns to the heart [O'Brien et al. [1997]]. During surgeries where a heart-lung machine is used, the heart is emptied of blood, and then refilled while using a method to get all the air out of the heart. There are multiple ways this can be done, and they can lead to different amounts of bubbles passing into the arteries and moving towards organs in the body. By monitoring exactly when and where bubbles appear, and how many, it can be possible to connect them to events during the surgery and possibly see what methods of filling the heart with blood leaves the fewest air bubbles. This project also considers patients going through catheter interventions to fix heart defects, where a heart-lung machine is not used. Monitoring of the blood flow could explain what procedures causes bubbles here as well.

## 2.2 Ultrasound Technology

The type of ultrasound technique relevant to this project, is diagnostic ultrasound [NIH [2016]]. It is a non-invasive method to image the inside of the body using transducers, or probes, that send out high frequent sound pulses. A subsection of diagnostic ultrasound called functional ultrasound can provide information maps to visualize changes in the organ structure. This is done by observing the velocity of tissue and blood inside the body, which is used in this project.

In an ultrasound system, the transducers produce waves and send them into the body (or other material), and detect them when echoes are reflected back. A special ceramic crystal called piezoelectric materials usually make up the active elements of ultrasound transducers. They have the necessary properties due to their ability to both produce sound waves when an electric field is applied, and produce an electric field when a sound wave hits [NIH [2016]]. When using this type of materials in an ultrasound scanner, the sound waves propagate through the body before being reflected by boundaries between the tissues. This generates electrical signals that are sent to the ultrasound scanner while calculating the distance between the transducer and the tissue boundary using the speed of sound. With this information, 2D-images can be made of the tissues and organs to search for deviations inside the body.

### 2.2.1 Ultrasound Doppler

Common ultrasound imaging looks at still images of the inside of the body. A technique important to this project that images the blood flow through blood vessels or organs, such as the heart, is ultrasound Doppler [MedlinePlus [2019]]. This method uses ultrasound technology with the Doppler effect to measure sound waves reflected from red blood cells in the arteries, or other matter, to capture movement.

There are two types of ultrasound Doppler - Continuous Wave (CW) and Pulsed Wave (PW) Doppler. CW Doppler continuously emits ultrasound waves that are analyzed when reflected [ecgwaves.com [a]]. This is done by using one piezoelectric crystal to emit, and one to reflect instead of using the same crystal for both. In this project, PW Doppler was used. Rather than sending continuous waves, PW Doppler uses short pulses of ultrasound that are analyzed between the pulses when reflected [ecgwaves.com [b]]. By doing this, the Doppler phase shift can be compared from pulse to pulse. PW Doppler also makes it possible to separate the signal in different depths from the probe.

Even though blood signals are weaker than those of other tissues, the movements can be extracted using ultrasound Doppler. Blood signals are normally high frequent, while clutter, consisting of signals of other tissues and noise, reverberations, and echoes, is usually at lower frequencies [Støylen]. In order to attenuate the low frequency clutter, while letting through the weaker high frequency blood signal of interest, a high pass filter can be used.

Blood flow can be observed by using Colour Doppler. By making an image of the blood flow using colours on a computer, the direction of the blood flow, and for instance air bubbles, can be shown with red for movement in one direction and blue for the opposite. From this, the velocity of the blood can also be found. Figure 2.1 shows the m-mode, or motion mode, image of a blood signal with bubbles in multiple depths at

the same time.

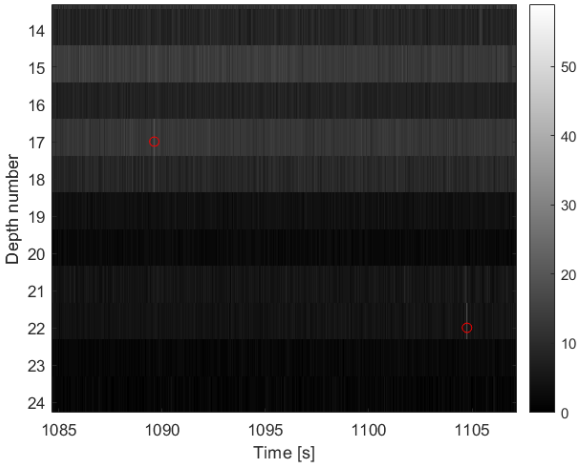


**Figure 2.1:** Motion mode ultrasound image of blood signal with bubbles

There are two examples of bubbles in figure 2.1 marked by red circles; one in depth 22 and one in depth 17. They can be separated from the rest of the IQ-signal by their lighter colour, due to higher intensity as the air bubbles reflect more of the ultrasound beam than the blood signal. They are also oblique, stretching in time and depth. The faster the bubble moves through the ultrasound beam of the transducer, as explained with figure 2.2, the steeper is the oblique line.

## 2.3 Doppler Signal from Bubbles

When using an ultrasound Doppler system, the blood flow can be measured continuously by placing the probe above an artery. The blood vessel, and also any air bubbles in the blood flow, might not pass the ultrasound beam at a 90° angle. The angle, $\varphi$, of the bubble's path through the beam can be used to calculate the velocity of the bubble provided one knows the diameter of the ultrasound beam. Figure 2.2 shows a rough example of this with the ultrasound transducer on top with a 10 mm diameter. The bubble is in this case assumed to be in the near field giving a beam diameter, $dt$, equal to the transducer's.

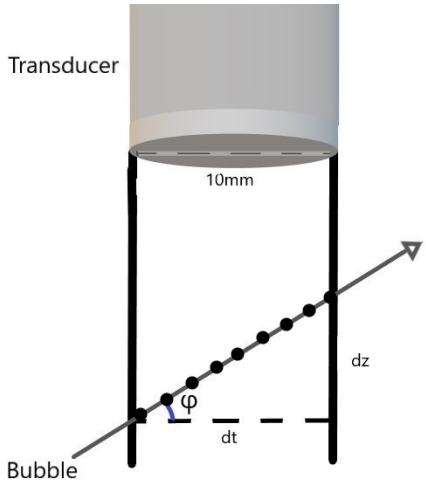


**Figure 2.2:** Transducer with a bubble crossing the ultrasound beam

Each dot on the trajectory of the bubble shown by an arrow depicts the echo that is returned for each pulse of the ultrasound beam. The bubble will send an echo back to the transducer for each pulse it is placed inside the beam. An example of an echo signal for a bubble in one depth is shown in figure 2.3.

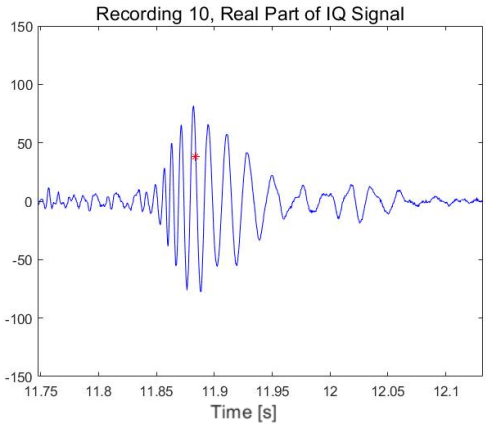


**Figure 2.3:** Doppler signal of bubble and blood

In this figure, the bubble is marked with a red star at its maximum intensity. It has roughly 10 periods of oscillation, which was chosen for the transmitted pulse, and the amplitude is larger than the surrounding blood signal. This shows how the Doppler signal of a bubble can be recognisable compared to that of blood.

## 2.4 Acoustics

In order to calculate scatter of sound waves from air bubbles in the blood stream, like ultrasound signals being reflected, the bubble can be modelled as a linear oscillator [Hoff [2000]]. For this to be true, the oscillation amplitude has to be small compared to the equilibrium radius of the bubble, which will be discussed in the next section.

### 2.4.1 The Resonance Phenomena

Bubbles in water, and in blood, are powerful ultrasound scatterers that can be seen as harmonic oscillators, as described by Minnaert in *On musical air-bubbles and the sounds of running water* [Minnaert [1933]]. This view explains the resonance frequency characteristic to oscillating bubbles under linear conditions. The resonance phenomena of small bubbles in blood is described in the book *Advances in Biomedical Measurement* [E. R. Carson and Krekule [2012]]. When small bubbles are in an ultrasound field, they start to vibrate. The relation between the bubble radius and the resonance frequency $f_0$ is given by

$$f_0 = \frac{1}{R_0}\sqrt{\frac{3\gamma\bar{P}_i}{\rho_0}} \tag{2.1}$$

where $R_0$ is the resonance radius of the bubble, $\bar{P}_i$ is the average pressure inside of the bubble, $\gamma$ is the specific heat of gas and $\rho_0$ is the density of blood [E. R. Carson and Krekule [2012]]. This can be used to find the bubble size if the other parameters are known. For example, the resonance frequency of the data in this project is $f_0 = 7.8$ MHz, so the radius of each bubble is relatively small. As long as the radius of the bubble is smaller than the wavelength of the ultrasound signal, the pressure surrounding the whole bubble will oscillate around a mean value given by the resonance radius [Hoff [2000]]. This means that if the pressure increases, the bubble will become smaller, while if the pressure decreases, the bubble will grow in size.

In order to consider bubbles in blood as linear oscillators, which is a much used model, the oscillation amplitude needs to be small in comparison to the equilibrium radius [Hoff [2000]]. The liquid surrounding the bubble also has to be displaced for the bubble to oscillate. This adds inertia to the system, and the liquid mass can be viewed as the mass of a mechanical oscillator, or the inductor of an electrical oscillator. This image can also be used when looking at the gas in the system and how the gas pressure acts like a spring. The gas compresses and expands which makes a spring force act against the change in volume, introducing resistance and dampening into the system.

### 2.4.2 Stiffness of Bubbles

Compression usually does not include heat transport in acoustics, but this does not apply to all bubble diameters and frequencies [Hoff [2000]]. The compression and expansion of a bubble can be compared to that of a spring with a weight, given by Hooke's law with a spring constant $s = 12\pi a\kappa p_e$. Here $a$ is the radius of the bubble, and $\kappa$ is the adiabatic constant $\gamma$ of the gas for adiabatic oscillations, no heat is transferred, or 1 for

isothermal oscillations, where heat is transferred to obtain a constant temperature. It is generally a function of bubble radius and sound frequency, while $p_e$ is the equilibrium pressure inside the bubble. This does not, however, consider the surface tension of the bubble or the effect of a shell encapsulating it as it is in blood, which will both increase the stiffness of the bubble [Hoff [2000]]. A surface tension will increase $p_e$ to

$$p_e = p_0 + \frac{2\tau}{a} \tag{2.2}$$

where $p_0$ is the hydrostatic pressure in fluid and $\tau$ the surface tension. The surface tension is much lower in blood than in water due to blood containing surface active protein molecules [Hoff [2000]].

### 2.4.3 Backscattering of Bubbles and Blood

The backscatter coefficient is defined as the scattering cross section per unit volume, when the scattering angle is 180° [Nam et al. [2011]]. The scattering cross section varies with frequency and diameter [Hoff [2000]]. For frequencies, $f$, a lot lower than the resonance, the scattering cross section increases by $f^4$. For higher frequencies, the cross section is independent of the frequency and is very different from the Rayleigh scatter. For bubbles with a smaller diameter than the resonance diameter, the scattering cross section will increase with $d^{16}$, where $d$ is the diameter. If the diameter is larger than the resonance, the scattering cross section increases with $d^2$.

When the concentration of bubbles is relatively low, like in this project, the oscillations from different bubbles do not interact [Hoff [2000]]. Because of this, and the fact that the power a bubble suspension absorbs is the sum of the total power absorbed by each bubble, the expression for the scattering cross section $\sigma_s(a_e,\omega)$ is given as equation (2.3) where $a_e$ is the equilibrium radius of the bubble.

$$\sigma_s(a_e,\omega) = 4\pi a_e^2 \frac{\Omega^4}{\left(\Omega^2-1\right)^2+\Omega^2\delta^2} \tag{2.3}$$

$\Omega$ is the angular frequency given as $\Omega = \frac{\omega}{\omega_0}$. $\omega = 2\pi f$, where $\omega_0$ comes from the resonance frequency, $f_0$, in equation (2.1). This equation gives the scattering cross section in every direction of every solid angle. It is the energy emitted in total of every direction of each bubble. For this project, only one direction is of interest; the backscattering cross section towards the ultrasound transducer as explained in section 2.3. Assuming the energy is emitted equally in all directions, the total scattering cross section can be divided by the solid angle, in the case of a circular bubble; $4\pi$. This gives the backscattering cross section in equation (2.4).

$$\sigma_s(a_e,\omega) = a_e^2 \frac{\Omega^4}{\left(\Omega^2-1\right)^2+\Omega^2\delta^2} \tag{2.4}$$

For the bubbles considered in this project, the resonance frequency is very large, so the bubble sizes are relatively small. Therefore, assuming $f$ is much larger than the resonance frequency, $f_0$, $\Omega$ is very large which means equation (2.4) can be simplified by dividing each element by $\Omega^4$. The resulting equation is shown in (2.5).

$$\sigma_s(a_e,\omega) = a_e^2 \frac{1}{1-\frac{2}{\Omega^2}+\frac{1}{\Omega^4}+\frac{\delta^2}{\Omega^2}} \tag{2.5}$$

This makes the fraction in equation (2.3) go towards 1 for large Ω, so equation (2.6) can be used for the backscattering cross section.

$$\sigma_s(a_e,\omega) = a_e^2 \tag{2.6}$$

In bubbles, the backscattered cross section, found from the resonance formula, can be estimated as $\sigma_{bubble} = \frac{1}{4}D_{bubble}^2$, where $D_{bubble}$ is the bubble diameter ($D_{bubble} = 2a_e$). The backscattered cross section of blood can be estimated as $\sigma_{blood} = \epsilon \cdot V_{blood}$, where $\epsilon$ is the backscatter coefficient given by equation (2.7) [Cobbold [2007]].

$$\epsilon = \epsilon_{1(HCT)} \cdot f_0^4 \tag{2.7}$$

$D_{bubble}$ is the diameter of the bubble, while $V_{blood}$ is the blood volume. HCT stands for hematocrit, meaning the percentage volume level of red blood cells in the blood [Evensen [2020]]. For normal hematocrit levels, $\epsilon$ is given as $\epsilon_{(HCT=40)} = 7 \cdot 10^{-4}$.

Equation (2.8) shows the emboli to blood ratio, $EBR$.

$$EBR = \frac{\sigma_{bubble}}{\sigma_{blood}} = \frac{1}{16\epsilon v_{blood}} \cdot D_{bubble}^2 \tag{2.8}$$

where $v_{blood}$ is the sample volume, which leads to the expression

$$D_{bubble}^2 = 2\pi c N f_0^3 \epsilon_1 \frac{D_v^2}{N \cdot \cos\Theta} EBR \tag{2.9}$$

where N is the number of bubbles in the sample volume, giving an expression for the size of the bubbles if the emboli to blood ratio is known. $c$ is the speed of sound, Θ is the scattering angle, while $D_v$ is the complete volume diameter. The bubbles are transient signals of high intensity, and have very different traits to blood and soft tissues. Because of the difference in density and speed of sound in the bubbles, they will have much more backscattering than the rest of the signals. This is because ultrasound signals are reflected most at the transition from one medium to another with different densities [Lønnebakken et al.]. Therefore, air bubbles can be distinguished from the surrounding blood and tissue signals like in this project, as shown in figure 2.3.

The diameter of the bubble, $D_{bubble}$, can be used to determine how dangerous a bubble could be [Hoff [2000]]. Larger bubble size increases the risk of stopping the blood flow through the artery. By calculating the bubble size of each bubble, smaller and less dangerous bubbles can possibly be disregarded while the larger ones are detected.

In order to determine the relative bubble size in this project, the maximum emboli, or bubble, amplitude to background amplitude ratio (EBR) was found. Both the bubble amplitude and the background signal amplitude are in dB, so the ratio is found by subtracting the background amplitude from the bubble amplitude. From this, the relative bubble size, and how much larger the bubble amplitude is than the background signal in dB is found.

### 2.4.4 The Doppler Equation

The Doppler effect, or the Doppler shift, is the change in sound frequency due to a reflector moving towards or away from the source [Murphy et al.]. One example is an ultrasound beam with a bubble moving in the blood stream. The Doppler equation that is used to calculate the Doppler shift is given in equation (2.10) [Murphy et al.].

$$\Delta f = \frac{2 f_0 \cdot v}{c} \tag{2.10}$$

where $\Delta f$ is the Doppler shift, $f_0$ is the frequency that is sent out, $v$ is the velocity along the ultrasound beam, and $c$ is the ultrasound velocity in blood given as 1570 m/s [Nave [2016]]. From the Doppler shift, the expected length of a bubble in time can be calculated which is useful to the algorithm developed in this project.

### 2.4.5 Signal Processing

A block diagram of the full signal chain until the power signal that is used in the algorithm is shown in figure 2.4, with inspiration from [Devi and Asokan [2014]].

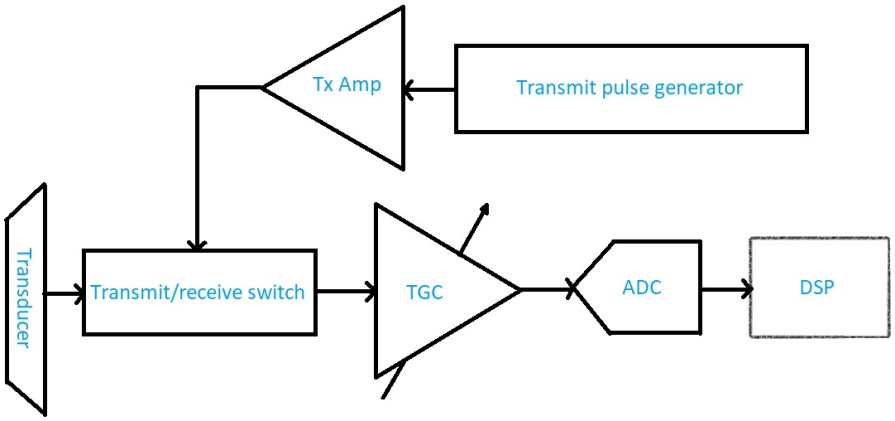


**Figure 2.4:** Block diagram of the full signal chain

In the block diagram in figure 2.4, the transmit pulse generator first generates a transmit pulse that will be sent from the front end part of the ultrasound system. The next block, Tx Amp, amplifies the transmit pulse before it is sent to the transmit/receive switch. The switch first sends the amplified transmit pulse to the transducer, and when it receives it once more from the transducer, which transmits the signal and receives the reflected one by converting electric signals to acoustic pressure waves and vice versa, it sends the received signal from the transducer to the TGC block. TGC is short for Time Gain Control or Time Gain Compensation. It compensates for the depth and reflections of the transmitted signal. The ADC block is the Analog to Digital Converter, which converts the signal from analog to digital for further signal processing. Next, signal pro-

cessing is done to the signal digitally which is also where the algorithm developed in this project comes in.

### Autocorrelation

The autocorrelation of a time series is the degree of similarity between the time series itself and a lagged version of the same series over a time interval [Proakis and Manolakis [2014]].

In the algorithm developed in this project, an estimate of the autocorrelation of each bubble was used to calculate the Doppler shift, and from this, the expected length of a bubble signal. The Doppler equation, equation (2.10) shows the function used to find the expected length given by

$$l_{expected} = abs\left(\frac{10}{\Delta f}\right) \tag{2.11}$$

where $\Delta f$ is the Doppler shift and $l_{expected}$ is the expected length of a certain bubble. 10 divided by the Doppler shift comes from the fact that the transmitted pulse was set equal to 10 cycles. The reflected bubble signals will therefore also have 10 periods of oscillations.

An estimate of the autocorrelation function can be used to find an approximate velocity of the bubble, which is used to find the Doppler shift and can be seen in equation (2.12) [Lai et al. [1997]] where $prf$ is the pulse repitition frequency.

$$v = \frac{c \cdot prf}{4 f_0 \cos\theta} \tag{2.12}$$

### Filtering

In this project, the cerebral blood flow was measured using ultrasound Doppler. The reflections from bubbles generally have higher intensity than blood, which makes it possible to differentiate the two by setting a threshold. Some parts of the IQ-signal, consisting of reflections from blood and noise, might exceed the threshold and be confused as bubbles. A low pass filter (LPF) was used to smooth out the background blood signal without affecting the bubble signal too much. It will let the parts of the signal with frequencies below a cutoff, the bubble signals, pass through untouched while dampening higher frequencies.

The noise can come from a variety of different sources and it is important that the actual signal is not altered, as dampening or distortion is a possibility. Another effect of filtering is lower peak values and time delays. There are different low pass filters to choose from depending on the purpose. A Butterworth filter, an infinite impulse response (IIR) filter, with an order as low as possible can be used. Low pass Butterworth filters are all-pole filters characterized by the magnitude-squared frequency response [Proakis and Manolakis [2014]]. This is given by equation (2.13), where N is the filter order.

$$|H(\Omega)|^2 = \frac{1}{1+(\Omega/\Omega_c)^{2N}} = \frac{1}{1+\epsilon^2(\Omega/\Omega_p)^{2N}} \tag{2.13}$$

In equation (2.13), $\Omega_c$ is the -3 dB frequency of the filter, and $\Omega_p$ is the pass band edge frequency. For the best possible results, the filter should have a flat pass band where the wanted signal is so that the complete signal will be passed through the filter without any dampening or distortion. A finite impulse response (FIR) filter will give the best phase response as it has a linear phase, but an IIR Butterworth filter has less latency, which might be the best choice if the system is to be used in real time.

Another type of filtering used in this project to estimate a threshold to separate the bubble signals from the blood is median filtering. By using the MATLAB function *medfilt1()*, an nth order one-dimensional median filter was applied to the dB power signal to get an approximate background signal based on the closest values of the signal [MathWorks [2020]]. This will avoid the overall background signal getting too high due to artifacts or other high intensity signals, and will make the bubble signals stand out more. The maximum bubble amplitudes were compared to the background amplitude just before the bubble in the EBR. The threshold was set a certain number of dB above the background which will be discussed in the next chapter.

## 2.5 Artifacts and Noise Signals

Different types of noise signals can interfere with the wanted bubble and blood signals in ultrasound imaging. Electromagnetic noise provides signals similar to that of a bubble with higher intensity than the surrounding blood signal. The noise can come from electromagnetic waves in the room, picked up by the patient's body, or be from high frequent medical instruments like electric knives. In these cases, the signals last for a longer time, but there are also shorter electromagnetic noise sources.

It is difficult to know what causes the momentary noise signals, but common for all electromagnetic noise is that it is independent of the ultrasound pulses and can be seen in all or most depths of the ultrasound image, something a bubble cannot [Ringelstein et al. [1998]]. There is also a second type of noise that can impact the recordings. If the ultrasound probe is not completely stable during the measurement, the Doppler shift of all depths will be detected due to the movement. This will also be seen in all depths, especially the earliest ones.

An example of artefacts, likely from using an electrical knife during surgery, is shown as horizontal lines in the right figures of figure 2.5, or to the far left of the left figures. The software this is from will be presented in the next chapter.

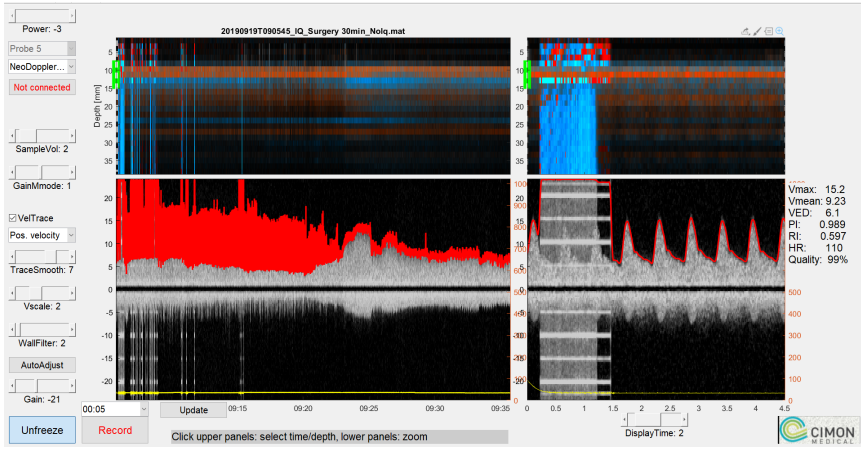


**Figure 2.5:** Example of artefacts

Chapter 3

# Methods

In this chapter, the methods used will be described. This includes the setup and data aquisition, including hardware and software, as well as the way to manually count bubbles, and the algorithm developed in this project. A simulation of blood signals was also made and used to test the algorithm on different types of data with varying numbers of bubbles in the earliest development stages.

## 3.1 Patients

This project focuses on detecting and counting bubbles, or emboli, in the brain of infants, but the used data sets come from two different sources. In all, 13 patients were young children going through heart surgery, while 18 were children going through a catheter intervention, but not all of them were analysed with the algorithm.

Air bubbles can come into the blood stream if a patient is connected to a heart-lung-machine, as for the children going through heart surgery in this data set. It is, however, not known for sure what induces these bubbles when the patient has a catheter intervention, where a heart-lung machine is not used. The individual cases are very different and involve many types of surgeries and interventions. All patients were, however, born with some sort of heart defect, or congenital heart disease.

### 3.1.1 Catheter Interventions

Among the 18 infants with a heart failure repaired by catheter intervention, a few suffered from pulmonary stenosis [Ritz [2017]]. This is a condition seen in young children where the pulmonary valve, a valve in the heart between the right ventricle and the pulmonary, or lung, artery, is too small, stiff or narrow to allow enough blood to pass through from the heart to the lungs. The treatment of this, which was performed while measuring the cerebral blood flow using the Doppler ultrasound system NeoDoppler, was to insert a balloon into the valve by using a catheter. Once the balloon was in the wanted position, it was inflated to open up the valve, leaving more room for blood to

flow through.

Another, in a way similar condition and intervention, is aortic valve stenosis [AHA [2020]], where the aortic valve in the heart is too narrow, preventing blood to pass through. This is, once again, solved by catheter intervention where a balloon is inserted into the valve to open up for the blood flow. This method was also done to infants suffering coarctation of the aorta [Holmström et al. [2019]]. This is a condition where the aortic arch is narrowed.

Some of the patients with heart conditions repaired by catheter interventions also had PDA, or Persisting Ductus Arteriosus [Clinic [2017a]]. PDA is a condition where there is a persitent opening between the two main blood vessels of the heart. This opening is called the ductus arteriosus, and usually closes a short while after birth. If it does not close, it becomes PDA and can in some cases lead to blood flowing in the wrong direction. This causes overcirculation of the lungs and can cause heart failure.

There were also some patients with more complex heart failures among the data sets used. These conditions will not be discussed further, but were also repaired by a form of catheter intervention.

Due to bad recordings or conditions, among other things giving a weak artery signal, catheter intervention patients 1 and 18 had to be taken out. No recordings of these two patients will be considered in the analysis.

### 3.1.2 Open Heart Surgery

The remaining 13 infants had open heart surgery to repair different kinds of heart failure. Multiple of these had AVSD, Atrioventricular Septum Defect, which means there is a hole in the wall between the atriums and between the heart chambers [Clinic [2019]]. This is accompanied by a valve deficiency, and can be repaired by closing the holes with a Gore Tex patch. It is, however, usually fixed by using the pericardium, a sac containing the heart [Wikipedia [2020]], of the patient. It is also resolved by sowing the atrioventricular valve. A longer recording was used to improve the algorithm developed in this project in its last stages. The patient of this recording suffered from AVSD which was closed by a Gore Tex patch between the chambers and a pericardium patch between the atriums. The system was also sown so that big leakages were avoided.

Some of the patients suffered VSD, Ventricular Septum Defect [Clinic [2017b]], which means the problem is a hole in the wall between the two lower heart chambers. This leads to blood being pumped back into the lungs instead of out to the rest of the body, which means the heart needs to work harder. This was solved by closing the hole using a Gore Tex patch like before. Another condition some patients suffered from was TGA [CCHMC [2019]], Transposition of the Great Arteries. This involves that the main artery and the lung artery (pulmonary) have switched places. The open heart surgery to fix this is an "arterial switch", meaning the arteries are moved to their usual spot, while also moving the coronary arteries to their correct place.

Open heart surgery while monitoring the cerebral blood flow was also done on infants with total anomalous pulmonary venous return [Mai et al. [2019]]. With this condition, the veins that drains the oxygen filled blood from the lungs to the left atrium are wrongly connected. This drains the blood to the right side of the heart instead. The surgery fixes this by connecting this to the left atrium. Once again, as for the catheter

intervention patients, some suffered from coarctation in the aortic arch. In this case, it was repaired by cutting the narrow area and then reconnecting the same vein.

Another condition among the patients was tetralogy of Fallot [Clinic [2017c]], a heart condition which is a combination of four defects. These are pulmonary valve stenosis as described in the catheter interventions section, ventricular septum defect like mentioned above, overriding aorta, meaning the aorta is shifted slightly and is positioned just above the ventricular septum defect, and right ventricular hypertrophy. The last is a condition where the muscular wall of the heart thickens due to working too hard. Tetralogy of Fallot is repaired by filling the hole and extending the outlet in the right side of the heart by cutting out muscle beams and possible using a patch to extend the pulmonary vein.

## 3.2 Setup and Data Aquisition

The data used in this project are from neonates during heart surgery and catheter intervention as presented above. A newly developed ultrasound technology system with an accompanying software was used to obtain the data, and will be described in the following subsections.

### 3.2.1 Ultrasound System - NeoDoppler

The data was obtained using a new ultrasound technology for continuous measurements of cerebral blood flow in neonates, called NeoDoppler [Vik et al. [2019]]. NeoDoppler aims to reduce the incidence of brain injury in premature infants and critically ill neonates by monitoring of the cerebral blood flow.

The instrument works by placing an ultrasound probe on top of the open fontanelle on the head of the neonate. This way, the cerebral blood flow can be measured continuously while being out of the way. NeoDoppler uses ultrasound Doppler as described in section 2.2.1, and has been developed by Professor Hans Torp and the Ultrasound Group at the Department of circulation and medical imaging at NTNU.

The system consists of three main components; an ultrasound probe connected above the fontanelle on the baby's head, an ultrasound module with power supply, and a computer with software for processing and displaying the data. The software, also developed at the Department of circulation and medical imaging at NTNU in collaboration with NTNU Technology Transfer [Nguyen [2019]], will be described in the next section.

### 3.2.2 Software - EarlyBird

The software developed for the NeoDoppler ultrasound system is called EarlyBird, and version 5.26a was used in this project. It obtains the raw data from the probe and scanner to process, and then presents it as a Doppler spectrum to be analysed. Different vessels can be chosen by choosing the depth of the focal point, and the gain and parameters used for filtering are adjustable [Jarmund [2019]]. EarlyBird also gives the opportunity to, among other things, search for bubbles or emboli in the blood flow in

multiple depths at the same time, which is useful to recognise bubbles that appear in different depths at different times or that stretches in time or depth. It also makes it possible to see if an artery has gone in and out of the image during the recording, which could possibly make the same bubbles be counted multiple times in different depths or times. An example of what a data set showing bubbles in a bloodstream looks like is shown in figure 3.1.

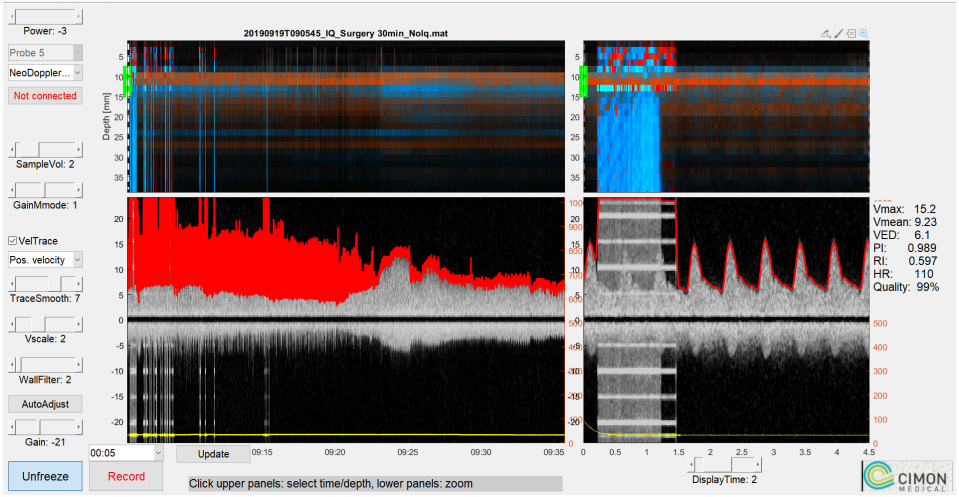


**Figure 3.1:** Color Doppler image of blood stream showing multiple bubbles in EarlyBird software

In figure 3.1, the top windows show the color m-mode image of the blood stream near the heart of a child during heart surgery. All yellow circles in the top left image mark manually counted bubbles. The signal is zoomed in on a smaller segment in the windows on the right hand side. Here it is easier to see how bubbles stand out from the surrounding blood signal. As described in section 2.2.1 about color Doppler ultrasound imaging, blue and red display movement in opposite directions of the artery. The blue and red oblique lines are clearly different to the rest of the image and are probably bubbles. If in doubt, the bottom window can be used. This shows the intensity of the signal, and the gain can be altered as needed. Around where the oblique lines can be seen in the top right image, the bottom right figure shows white parts in the otherwise grey signal. Again, this indicates the presence of bubbles. The bottom left figure depicts the Doppler spectrum.

## 3.3 Manual Counting of Bubbles

After getting data using NeoDoppler and EarlyBird as previously described, the counting of bubbles has been done manually at St. Olavs Hospital. Oblique red or blue lines depicting bubbles are marked by clicking them in the EarlyBird interface. When the whole signal has been checked and all detected bubbles are marked, the total number of bubbles are counted. Figure 3.1 shows a quite clear example, but the difference

between bubbles and blood might not always be as obvious. It is also difficult to see if only one bubble is present, or multiple close by each other. If enough bubbles are in the same area, they are counted as a cloud or curtain of bubbles without a specific number. In order to get a number of bubbles as correct as possible, the same data sets need to be counted multiple times, and may be checked by multiple people which is very time consuming. This is why, as previously mentioned, an automatic algorithm for embolic detection would be an advantage.

## 3.4 Simulation

Simulated blood signals were used to get data sets with a known number of bubbles and clouds of bubbles for control. The blood and bubble signals were simulated to act as similar to real IQ-signals as possible, including a random blood signal and chosen bubble signals in different depths and time. The same sampling frequency and other variables are used as in the real signals obtained from Rikshospitalet. The code for this, made by Hans Torp, is given in the appendix.

The code is written in MATLAB, and first sets important parameters to the same as the original ultrasound system used for the recordings, such as the ultrasound speed in blood, $c$, and the frequency, $f0$. The center point of trajectory for every simulated bubble is adjustable, and the number of bubbles is chosen by the user who can add and remove them at will. This makes the signal more accurate to the original recordings, and gives the option of multiple bubbles close together or in different depths, times, and with different trajectory center points.

Clouds, or curtains, of bubbles can be added to the simulated signal together with the background blood signal and single bubble signals. The clouds can be placed anywhere and consist of a lot of randomly distributed bubbles given the start time and duration of the cloud set by the user.

After all wanted bubbles and clouds are placed, the blood and bubble signals are convoluted before the total signal is displayed. The thermal noise, which should be included to better simulate a real life environment, is set by randomized vectors of the same length as the IQ-signal. The total IQ-signal including the thermal noise is then calculated before plotting the signal using a grayscale colormap. These signals were used in the first stages of the algorithm development to see how well the algorithm detected a controlled set of data.

## 3.5 Algorithm for Automatic Detection of Embolis

The training set consisted of four recordings with bubbles and 12 without and was used to adjust the different parameters in the algorithm for best possible detection. Other, shorter recordings were also used in the early stages of the algorithm development. Two of the recordings were from the same patient at different times and will be referenced as pilot recording 1 and 2. Due to its number of bubbles and the length of the recording (30 minutes), pilot recording 1 was mostly used to develop the algorithm before the final testing. It will therefore mainly be used in examples. An overview of the complete

algorithm is shown in figure 3.2 with the most important inputs and outputs. The different parts of the algorithm will be presented in this chapter, and the functions, in boxes with thicker edges, will be described in detail.

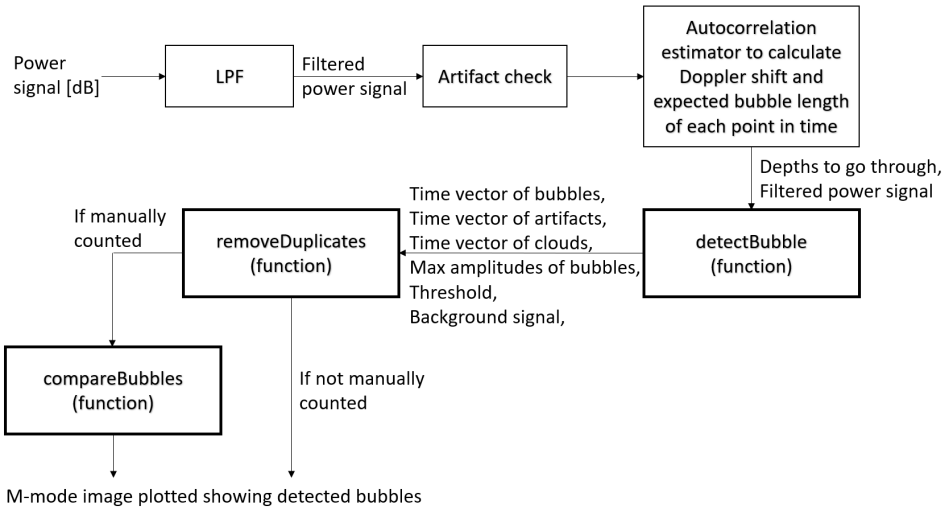


**Figure 3.2:** Overview of the Automatic Detection Algorithm

The automatic detection algorithm developed in this project uses the power signal straight from the EarlyBird software. It is developed to go through one depth at a time, through all depths chosen by the user. If multiple depths are chosen, a correction algorithm will correct duplicate detections of bubbles. This is described in section 3.5.2. Before the bubble detection can start, the complete power signal of the recording is filtered using a $2^{nd}$ order Butterworth LPF. The indexes of the signal containing artifacts are then found. These are higher intensity noise signals due to medical instruments or other causes that are not bubbles as explained in section 2.5. All parameters that can be changed by the user will be presented in more detail with values chosen for the training set in section 3.5.4.

```
art_detect = zeros(1,length(cmmode.PdB));
for x = 1:n_artefact
    Pow_dB = pow_dB(x,:); %Power in dB for depth n
    Pow = 10.^(Pow_dB/10); %Power in depth n
    bgs_dB = 10*log10(Pow); %Background signal
    thresh = median(bgs_dB) + thresh_var; %Threshold
    for a = 1:length(Pow_dB)
        if (Pow_dB(a) > thresh-1) && (a > artLim) && (a < length(Pow_dB)-artLim)
            art_detect(a) = 1; %This index is registered as an artefact
            art_detect(a-artLim:a+artLim) = 1; %Some artefacts are slightly oblique
        end
    end
end
```

To check if and where artifacts are present, the first depths of the m-mode image are

considered, the number of depths is chosen by user input *n_artefact*. Artefacts due to medical instruments stretch through all or most depths, and as the background signal is usually lower in the first depths, they are more clearly visible here. Another factor is that there usually are no arteries at the lower depths, only veins which are not that relevant for the bubble detection in this project. If a high intensity signal is detected in the lower depths, the index is registered as an artifact to be compared in the bubble detection by changing the value at this point in a vector from 0 to 1. If the index is registered as an artifact, any bubbles detected here will be disregarded as an artifact. It could also be done by checking if the signal stays above the threshold in multiple depths at the same index. This proved to be a poorer solution that still counted a lot of artifacts as bubbles and was therefore not used in the finished algorithm.

The Doppler shift is calculated using an autocorrelation estimator, as explained in section 2.4.5, to find an expected length of a potential bubble in each point in time. This is done to make sure no short spikes or clouds of multiple bubbles are counted as singular bubbles. The length of each potential bubble signal is therefore compared to the expected length and has to be within an interval around the expected length, set by the user.

The user chooses in which depths of the m-mode image to check for bubbles, and an approximation of the background signal is found by median filtering of the signal in each depth. The background signal is then converted to dB, and a threshold is set a certain number of dB above this, determined by the variable *thresh_var*.

### 3.5.1 Bubble Detection Function

The bubble detection is done inside a function called *detectBubble* in the algorithm shown in the appendix. In the MATLAB code just below, the bubble detection is done by first converting the power in the chosen depth from dB to be filtered using median filtering of length *N*. The background signal is the dB conversion of the filtered signal, giving the background amplitude of each point. The threshold is set a number of dB above the background signal with *thresh_var* chosen by the user.

```
1 function [bubble_bgs,bubble_amp,nbub,time_bubble,time_art,time_c,maxval,thresh,Pow,
      bgs_dB] = detectBubble(n,minLength,prevBub,cloudLength,N,Pow_dB,T,tIncr,t,
      art_detect,thresh_var)
2     Pow = 10.^(Pow_dB/10); %Power in depth n
3     Filtered = medfilt1(Pow,N); %Median filtering using every Nth point
4     bgs_dB = 10*log10(Filtered); %Background signal in dB
5     thresh = bgs_dB + thresh_var; %Threshold
6     %%
7     a = 1; num_art = 0; c = 0; cloud_count = 0; prev = 0; bubbles = 0;
8     time = zeros(size(t)); time_art = zeros(size(t)); time_c = zeros(size(t));
```

The input and output variables of the *detectBubble* function are presented in table 3.1 with descriptions. The input variables are placed above the double line, while the output variables are below.

**Table 3.1:** Input and output variables of the bubble detection function

| Variable | Description |
|---|---|
| n | The current depth in the for-loop |
| minLength | Minimum length of a bubble |
| prevBub | Minimum space between bubble detections |
| cloudLength | Maximum length of bubble before it is counted as a cloud |
| N | Length of the median filter |
| Pow_dB | The signal power in dB for the current depth n |
| T | A vector of expected length of each point in time, found from the Doppler shift |
| tIncr | Time increment of the signal |
| t | Time vector from the EarlyBird software |
| art_detect | Vector containing indexes of artifacts |
| thresh_var | The number of dB above the background signal the threshold is |
| bubble_bgs | Vector with background signals of detected bubbles |
| bubble_amp | Vector with maximum amplitudes of detected bubbles |
| nbub | Vector of the depth of detected bubbles to be added to vector containing all bubble depths |
| time_bubble time_art time_c | Vector with times of each detected bubble, artefact and cloud/curtain |
| maxval | Vector of maximum intensity of all bubbles and potential bubble signals |
| thresh | Vector of thresholds for current depth |
| Pow | Signal power for current depth |
| bgs_dB | Background signal in dB of current depth |

The next step in the algorithm is a for-loop going through every index of the dB power signal in the chosen depth. Following this, the number of indexes the power signal stays above the threshold is counted using a while-loop to find the length of the potential bubble signal. By looking at the signal segment above the threshold, the max-

imum value, and its index, is found based on the amplitude of the power signal at this point in time. They are then added to the vectors *maxval* and *maxind*. This is the maximum amplitude of the potential bubble signal, and its index, and can be used to approximate the relative bubble size by comparing it to the background signal of the first index of the bubble signal. The reason why the background signal is not taken from the index of the maximum bubble signal is that the background is not supposed to contain any bubbles, only the surrounding signal.

```
    for i = 1:length(Pow_dB)
        if i >= a
        b_length = 0;
        l_expected = round(T(n,i)/tIncr); %Expected length
        a = i; %Start index for possible bubble
            while (Pow_dB(a) > thresh(a)) && (a < length(Pow_dB)) %Finds how long
                 the signal stays above thresh + ending index
                b_length = b_length + 1;
                a = a + 1;
            end
            c = c + 1;
            [maxval(c),maxind(c)] = max(Pow_dB(i:a)); %index and value of max point
                 from i (start) to a (stops being above threshold)
```

To make sure this is not an artifact, the index of the maximum value is compared to *art_detect*. If *art_detect* contains 1 at this index, a variable counting artifacts adds one, and the time is added to a different vector containing artefact times.

```
            if (i < length(Pow_dB) - maxind(c)) && (art_detect(i + maxind(c)) == 1)
                time_art(i + round(maxind(c))) = t(i + round(maxind(c))); %To mark
                     artefacts in figure
                num_art = num_art + 1;
```

If the index of *art_detect* contains a 0, meaning no artifact was detected, a number of previous indexes, chosen with the *prevBub* parameter, are checked to see if a bubble has recently been detected. This is to avoid double detections of the same bubble in the same depth. If no bubbles are found, the length of the bubble signal is compared to the expected bubble length calculated from the Doppler shift. A new parameter, *cloudLength*, is used to decide the maximum length of a singular bubble before it is counted as a cloud. A counter adds 1 if it is detected as a cloud, while it is otherwise counted as a bubble if the length is larger than $l\_expected/minLength$, where *minLength* is a user input. The time of each bubble peak is saved in a vector to be plotted in an m-mode image.

```
            elseif (i < length(Pow_dB) - maxind(c))
                for k = 1:prevBub %To avoid bubbles very close together that are
                     probably the same one
                    if (i > k) && (time(i - k) ~= 0)
                        prev = 1;
                    end
                end
                if (b_length > cloudLength*l_expected) && (prev == 0) %Minimum
                     length of cloud
                    cloud_count = cloud_count + 1;
                    time_c(i + round(maxind(c))) = t(i + round(maxind(c))); %To mark
                         clouds in figure
```

```
10                  elseif (prev == 0) && (l_expected > 0) && (b_length > l_expected/
                        minLength) %Minimum length for bubble
11                      bubbles = bubbles + 1;
12                      bubble_amp(bubbles) = maxval(c);
13                      bubble_bgs(bubbles) = bgs_dB(i);
14                      nbub(bubbles) = n;
15                      time(i + round(maxind(c))) = t(i + round(maxind(c))); %To mark
                            bubbles in figure
16                  end
17              end
18              short = 0; prev = 0;
19          end
20      end
21  end
```

The power signal in dB and the m-mode image is plotted with all detected bubbles marked with a *. In figure 3.3, a short part of pilot recording 1 in depth 17 is shown. The power signal in figure 3.3a shows the light blue dB power signal in this depth, with the black background signal, and the red threshold.

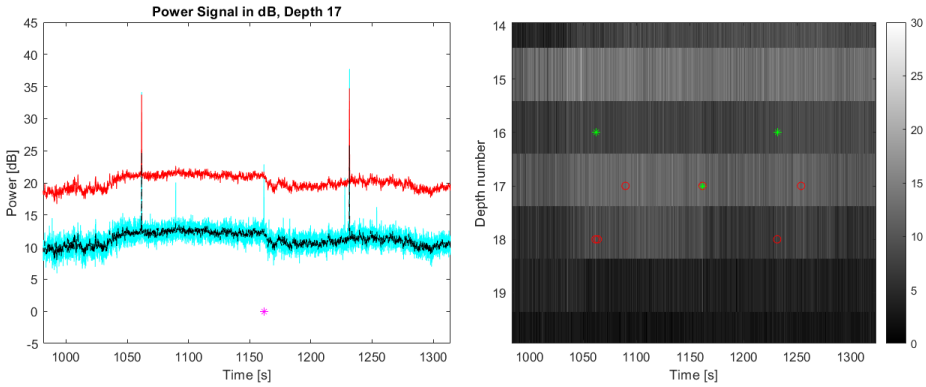


**(a)** Power signal in dB

**(b)** M-mode image

**Figure 3.3:** Example of pilot recording 1 in depth 17

There is only one marked bubble in figure 3.3a even though there seems to be three or four visible peaks above the threshold. From figure 3.3b it can be seen that two of these, the peaks around 1060 and 1240 seconds, have been detected in depth 16 and are therefore disregarded in this depth. The method of removing duplicate detections will be explained in section 3.5.2. The peak around 1100 seconds is not detected as a bubble as it is just below the threshold. The last bubble in depth 17, visible in figure 3.3b around 1250 seconds, is also below the threshold and is not detected by the algorithm in this depth.

### 3.5.2 Function to Correct Duplicate Detections

Because the algorithm was implemented to check individual depths, some bubbles are counted multiple times in different depths. To fix this, all detected bubbles are checked

afterwards to only include one of the duplicate detections in the results. The function is called *removeDuplicates* in the automatic detection algorithm in the appendix. The number of detected bubbles is also corrected. The input and output variables of the function are shown in table 3.2 with descriptions. Input variables are above the double line, while output variables are below.

**Table 3.2:** Input and output variables of the duplicate correction function

| Variable | Description |
|---|---|
| bubble_amp_all | Struct containing maximum amplitude of bubbles in all depths |
| bubble_bgs_all | Struct containing background signal of bubbles in all depths |
| nbub_all | Struct containing depth of bubbles in all dephts |
| time_bubble_all | Struct containing time of bubbles in all depths |
| n_start | First depth the algorithm checks |
| n_end | Last depth the algorithm checks |
| time_bubble_all | Updated struct containing time bubbles in all depths without the duplicates |
| bubble_amp_all | Updated struct containing maximum amplitude of bubbles in all depths without the duplicates |
| bubble_bgs_all | Updated struct containing background signals of bubbles in all depths without the duplicates |
| nbub_all | Updated struct containing depth of bubbles in all depths without the duplicates |

### 3.5.3 Comparing Manually Counted and Automatically Detected Bubbles

In order to evaluate how good the algorithm detects bubbles, the results of the training and test set were compared to manually counted bubbles. The full MATLAB code can be seen in the appendix as the function *compareBubbles* in the automatic detection algorithm. It uses for-loops to go through every detected bubble of the algorithm and compare each to the manually counted bubbles. If a bubble from the algorithm and a manually counted are close enough in time, less than half a second apart, and close enough in depth, maximum four depths apart, they are assumed to be the same bubble. A counter then adds one to a variable showing correctly counted bubbles.

If any bubbles in the vector containing the manually counted bubbles are not detected, each of them will be added to a counter showing missed bubbles. A vector containing the time of each of these bubbles is also updated, but will include some bubbles

that are detected in later depths. Detected bubbles from the algorithm that were not counted manually are added to a counter showing false detections, or false positives. The *compareBubbles* function is only run if the user input *manual* is equal to 1 as the algorithm is supposed to be used on recordings that have not been counted manually. The function is mainly used to evaluate how well the algorithm works. The input variables of the function are shown above the double line in table 3.3, while the output variables are below.

**Table 3.3:** Input and output variables of the comparison function

| Variable | Description |
|---|---|
| crange<br>figh<br>cmmode | Parameters to plot in the m-mode-image previously generated and get manually counted bubbles |
| n | The current depth |
| time_bubble | Vector containing time of bubbles in current depth |
| time_correct_all<br>time_fake_all<br>time_miss_all<br>time_corr_other_depth_all | Structs with time of correct, false, missed, and correct bubbles of other depths updated within the function |
| bubbles_correct<br>bubbles_fake<br>bubbles_missed | Number of correct, false and missed bubbles up to the current depth |
| bubbles_manual<br>bubbles_correct<br>bubbles_fake<br>bubbles_missed | Updated number of manually counted, correct, false and missed bubbles |
| time_correct_all<br>time_fake_all<br>time_miss_all<br>time_corr_other_depth_all | Updated struct containing time of correct, fake, missed and correctly detected bubbles of other depths in all depths so far |

### 3.5.4 User Inputs

There are a few parameters that can be changed by the user in a struct called *userVar*. These are presented in table 3.4 with the parameter name, description and value chosen for the algorithm based on the training set.

**Table 3.4:** User inputs of the algorithm

| Parameter | Value chosen for training set | Description |
|---|---|---|
| N | 100 (0.25 seconds) | Length of the median filter |
| thresh_var | 9 dB | Variable set by user, determines how many dB above the background signal the threshold is |
| n_start | 7 | The first depth the algorithm goes through |
| n_end | 24 | The final depth the algorithm goes through |
| $f_c$ | 20 Hz | The cutoff frequency of the LPF |
| n_artefact | 5 | The number of depths used to detect artefacts |
| artLim | 5 (0.01 seconds) | Points ± this value from a detected artefact will also be marked as an artefact |
| cloudLength | 40 | The maximum length of a bubble before it is classified as a cloud is the expected length multiplied by cloudLength |
| prevBub | 200 (0.5 seconds) | Variable to avoid bubble detections too close together |
| minLength | 2 | The minimun length of a bubble is determined by the expected length divided by minLength |
| manual | 1 or 0 | If equal to 1, the comparison function is run if equal to 0, the comparison funciton is not run |

The values in table 3.4 gave the best results of the training set as a whole but can be changed for other recordings. Although *thresh_var* = 9 dB still gave a few false and missed detections, it was the best compromise. The *manual* parameter can be set equal to 1 if the data set has been manually counted. The algorithm will then run the *compareBubbles* function and compare automatically detected bubbles to the manually counted ones, reporting on the number of correct, missed and false detections. This is mainly for testing and evaluation of the algorithm. There were no examples of clouds of bubbles in the training set. Therefore, the maximum length of a bubble was set as small as possible, seeing that no manual single bubbles were counted as clouds. A maximum bubble length of 40 times the expected length was the smallest limit that did not detect manually counted bubbles as clouds in the training set. This also gave correct cloud detection of shorter recordings used in the earliest stages of the algorithm devel-

opment.

The power signal was filtered using a Butterworth LPF in the beginning of the algorithm. Three different cutoff frequencies, $f_c$, each tested using four values of *thresh_var*, are presented in table 3.5 showing the total number of correct, false and missed detections of the training set.

**Table 3.5:** Results from the training set with different thresholds and filter cutoff frequencies

| $f_c$ $[Hz]$ | **thresh_var** | **Correct** | **False** | **Missed** | **Total number of detected bubbles** | **Total number of manually counted bubbles** |
|---|---|---|---|---|---|---|
| 10 | 8.0 | 54 | 8 | 44 | 62 | 98 |
| | 8.5 | 52 | 6 | 46 | 58 | 98 |
| | 9.0 | 50 | 4 | 48 | 54 | 98 |
| | 9.5 | 48 | 2 | 50 | 50 | 98 |
| **20** | 8.0 | 65 | 37 | 33 | 102 | 98 |
| | 8.5 | 64 | 21 | 34 | 85 | 98 |
| | **9.0** | **59** | **10** | **39** | **69** | **98** |
| | 9.5 | 52 | 6 | 46 | 58 | 98 |
| 30 | 8.0 | 69 | 51 | 29 | 120 | 98 |
| | 8.5 | 68 | 29 | 30 | 97 | 98 |
| | 9.0 | 63 | 17 | 35 | 80 | 98 |
| | 9.5 | 58 | 9 | 40 | 67 | 98 |

From table 3.5 it looks like $f_c$ = 20 Hz gave the most correct detections while keeping the number of false positives to a minimum. When testing the cutoff frequencies, only half steps of the threshold were used. To estimate a more precise threshold, values around *thresh_var* = 9 dB were tested as this seemed to give the best results in table 3.5. The results are shown in figure 3.6.

**Table 3.6:** Results from training set with more precise thresholds for $f_c$ = 20 Hz

| **thresh_var** | **Correct** | **False** | **Missed** | **Total number of detected bubbles** | **Total number of manually counted bubbles** |
|---|---|---|---|---|---|
| 8.8 | 60 | 15 | 38 | 75 | 98 |
| 8.9 | 59 | 13 | 39 | 72 | 98 |
| **9.0** | **59** | **10** | **39** | **69** | **98** |
| 9.1 | 57 | 8 | 41 | 65 | 98 |
| 9.2 | 56 | 8 | 42 | 64 | 98 |

A threshold 9 dB above the background signal seemed to provide the best results. This gave the same number of correct detections as 8.9 dB, but with three less false positives. It also resulted in two more correct detections than 9.1 dB, but with two more false positives. In all cases, the number of missed bubbles is quite high, but it is difficult to improve with the current algorithm without obtaining many false detections. Using these settings, maximum two bubbles were detected in the recordings containing no bubbles, whereas lower thresholds or a higher $f_c$ resulted in more false detections.

The given cutoff frequency, $f_c = 20$ Hz, provided the overall best results. Although more correct detections of bubbles were made in pilot recording 1 without a filter, more bubbles were also falsely counted. Figure 3.4 shows the unfiltered (top) and filtered using $f_c = 20$ Hz (bottom) power signal in dB and m-mode image of pilot recording 1 in depth 21.

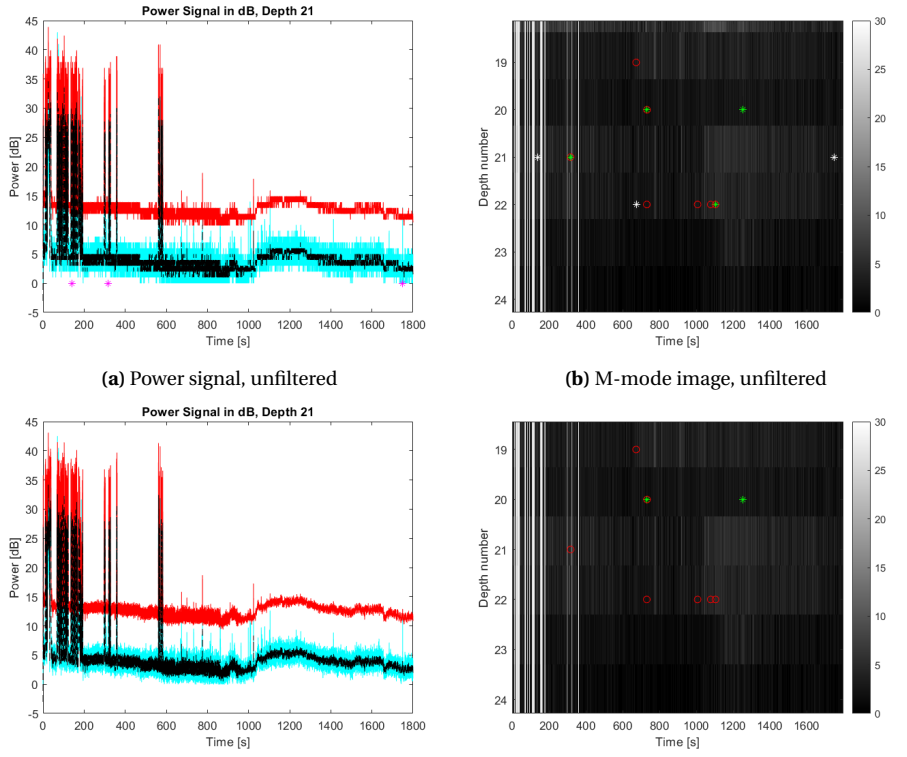


**(a)** Power signal, unfiltered

**(b)** M-mode image, unfiltered

**(c)** Power signal, filtered

**(d)** M-mode image, filtered

**Figure 3.4:** The effects of filtering on pilot recording 1

In the left figures, the filtered power signal is not that different from the unfiltered signal, but it is filtered enough to avoid a lot of false detections. Two examples of false detections in depth 21 of pilot recording 1 are shown in the m-mode image of the unfiltered signal in figure 3.4b. The bubbles are marked with pink * in the left figure. The two false detections in the unfiltered signal are not detected in the filtered signal which

can be seen in figure 3.4c and its m-mode image in figure 3.4d. In the m-mode images, a bubble is also falsely detected in depth 22 of the unfiltered signal while it is not detected in the filtered one. The filtered signal does, however, also miss two more correct bubbles in the part of the m-mode image shown in figure 3.4.

Chapter 4

# Results

## 4.1 Simulation

The simulation, that was previously mentioned and can be seen in full in the appendix, gives an overview of how the bubble and blood signals from a real patient might look. The simulated signals were used in the first phases of the algorithm development, before pilot recording 1 was used, and when the IQ-signal was analyzed instead of the power signal. An example of the resulting simulated IQ-signal, power signal and m-mode image with three bubbles is shown in figure 4.1.

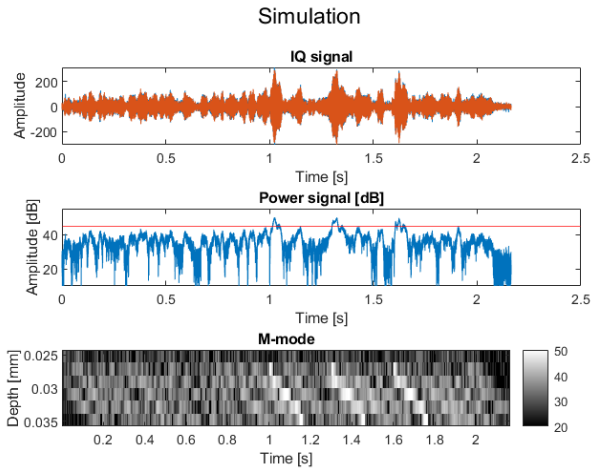


**Figure 4.1:** IQ-signal (top), power signal in dB with threshold (middle), and m-mode image (bottom) of a simulated signal

The top part of figure 4.1 shows the real (blue) and imaginary (red) parts of the total

IQ-signal plotted on top of each other. The IQ-signal includes the blood signal, thermal noise and the higher intensity echo of three bubbles. They all quite clearly have a larger amplitude than the surrounding blood signal in the top figure. In the middle figure, the power signal in dB of depth 3 (just before 0.03 mm) is shown. The amplitude is higher where the three bubble signals are, and are all above the red line giving an example of a suitable threshold for the simulation. In this case, the threshold is set equal to the same value throughout the signal, while it varies with a mean filter of the closest values in the actual algorithm. This was done because the newest version of the algorithm has been changed so much since the simulation was used that a lot of parameters were missing or had to be changed in order to run the algorithm on the simulated signal. The bubble signals can be seen as much lighter, oblique lines in the m-mode image at the bottom, moving slightly through time and depths. This is expected of the m-mode image of real life air bubbles in blood moving through the ultrasound beam. The lighter gray background simulates the blood signal from the m-mode image of the cerebral blood flow.

For comparison, similar plots are shown in figure 4.2 of pilot recording 1. Figure 4.2a shows the power signal in dB of one depth, while figure 4.2b is the corresponding m-mode image, similar to the one of the simulated signal.

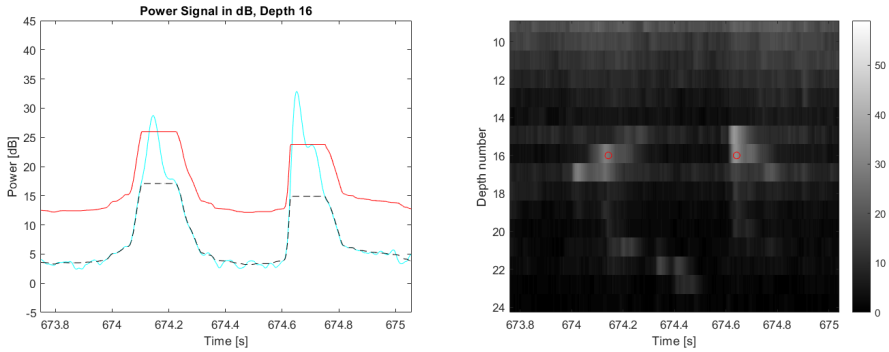


**(a)** Power signal

**(b)** M-mode image

**Figure 4.2:** Example of pilot recording 1

The recording in figure 4.2 is from pilot recording 1 in depth 16. Two bubbles are present, marked by a red circle in figure 4.2b, and are clearly different from the background blood signal. The light blue power signal in figure 4.2a reaches above the threshold in two places. The threshold is marked by a red line, while the black dotted line is the estimated background signal. This is a much more zoomed in image of the power signal than for the simulation, but shows the similarities. A power signal that is not zoomed in can be seen in figure 3.4 to compare the overall look of it. The bubble signals in the m-mode image shows the similarities between a real signal from a patient and the simulated signal, and how the simulation can be useful in development where the training set is quite small.

## 4.2 Results of the Training Set

The best compromise of the threshold was 9 dB above the background signal, as presented in section 3.5.4, which is used in all examples.

### 4.2.1 Pilot Recording

All recordings and data sets used up to this point were shorter signals of less than one minute while pilot recording 1 is 30 minutes long. The data set had been manually counted with 26 bubbles in total. The m-mode image of the full signal with marked bubbles is shown in figure 4.3.

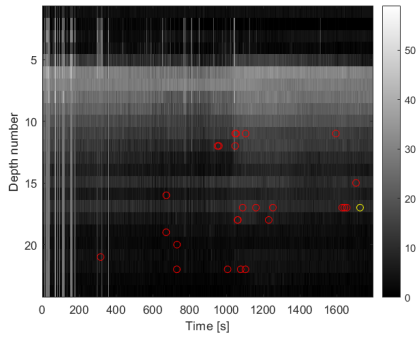


**Figure 4.3:** Manually counted bubbles marked by red circles in the m-mode image

In figure 4.3 multiple artifacts can be seen as lighter vertical lines, mainly in the beginning of the recording. These are most likely from a surgical electric knife used to cut open the chest of the patient to reach the heart for the operation. This leads to high intensity signals that exist in all depths of the ultrasound m-mode image as seen mainly from 0 to 400 seconds in the figure. The manually counted bubbles are marked in the m-mode image with red circles, while the yellow circle indicates an uncertain bubble, or a signal that might be a bubble, but is not clear enough to be counted for sure.

In pilot recording 1 there are no bubbles prior to depth number 11. The first 5 depths have a very low background signal intensity which can be used to identify artifacts as they stand out even more here than in the lower depths. The probability of finding bubbles in the earlier depths is quite small as there are mainly veins here and most bubbles are found in the arteries. It could also be more difficult for the algorithm to separate bubble signals from noise in these depths which can result in a lot of false detections. Because of this, the algorithm searches for bubbles starting at depth number 7. The depths the algorithm goes through can be changed manually for each data set.

#### Bubble Detection in All Relevant Depths Simultaneously

The automatic detection algorithm was run on the training set going through all depths from number 7 to 24. Because the algorithm checks each depth individually and counts

bubbles that might also be counted in a different depth, all detections had to be checked using the double detection function described in section 3.5.2. The resulting m-mode image of pilot recording 1 with manually and automatically marked bubbles is shown in figure 4.4a. The similar m-mode image of pilot recording 2 is shown in figure 4.4b.

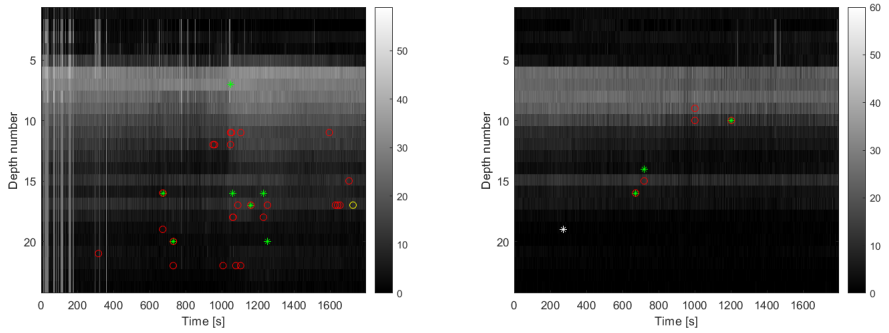


**(a)** Pilot recording 1

**(b)** Pilot recording 2

**Figure 4.4:** Results from pilot recording 1 and 2

Like before, the red circles are manually counted bubbles and the yellow circle is an uncertain, manually counted bubble. The green stars mark bubbles that are automatically counted correctly, and there are 7 in pilot recording 1. White stars depict falsely detected bubbles that are counted automatically but not manually. There are no false detections in pilot recording 1, but the algorithm missed 19 bubbles. Figure 4.4b shows there is one false positive, and two missed bubbles in pilot recording 2. It does, however, only have 5 manually detected bubbles in total where 3 were counted correctly. For comparison and to get a more complete picture, the results from the remaining recordings of the training set with bubbles are presented in figure 4.5.

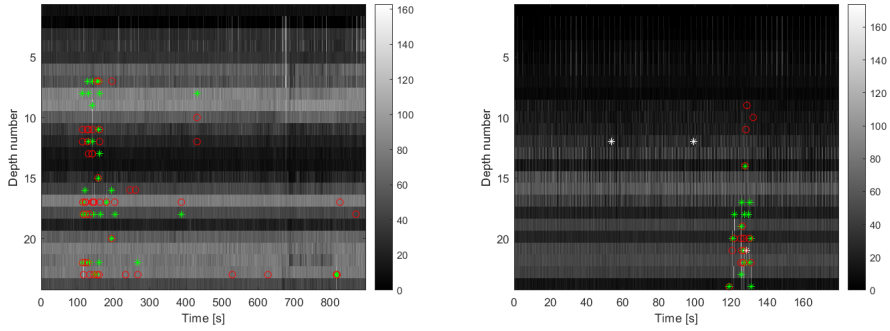


**(a)** Training recording 1

**(b)** Training recording 2

**Figure 4.5:** M-mode results of the remaining training set

There are no false positives in training recording 1, but in this case, 15 of the total

49 bubbles were missed. There are three missed detections in training recording 2, and three false. One of these is within the group of correctly detected bubble signals around 120 to 140 seconds. This is zoomed in and shown in figure 4.6 to be discussed in the next chapter. Figure 4.6 also shows two of the three missed bubbles in depth 9 and 11.

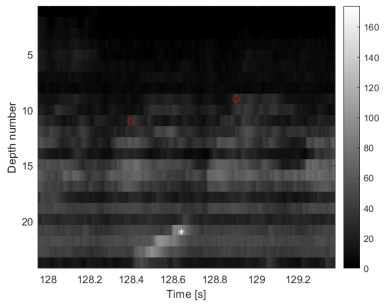


**Figure 4.6:** False bubble in training recording 2

Most of the falsely detected bubbles in the training set were due to movement artifacts. This is a type of artifact caused by movement of the probe or the structures that reflect the ultrasound signal, relative to the probe. A Doppler shift is then obtained in multiple depths at the same time that is usually strongest in smaller depths. A solution to the problem was not found during this project, but could be a possible improvement of the algorithm. By looking at multiple depths at the same time, and not each depth separately, false detections caused by movement could be avoided.

The number of bubbles counted correctly and missed, and false positives, are presented in table 4.1 for each depth of pilot recording 1. The missed detections will be discussed more in the next chapter. In total, 7 bubbles were detected automatically while there were 26 manually counted bubbles. The values are from using $thresh\_var = 9$ dB and a cutoff frequency of $f_c = 20$ Hz, which did not provide the best results in pilot recording 1.

**Table 4.1:** Results from pilot recording 1

| Depth | Correct | Missed | False | Comments |
|---|---|---|---|---|
| 7 | 1 | 0 | 0 | One bubble counted from depth 11 |
| 8, 9, 10 | 0 | 0 | 0 | No bubbles |
| 11 | 0 | 3 | 0 | |
| 12 | 0 | 3 | 0 | |
| 13, 14 | 0 | 0 | 0 | No bubbles |
| 15 | 0 | 1 | 0 | |
| 16 | 3 | 1 | 0 | Two bubbles counted from depth 18 |
| 17 | 1 | 4 | 0 | |
| 18 | 0 | 1 | 0 | |
| 19 | 0 | 1 | 0 | |
| 20 | 2 | 0 | 0 | |
| 21 | 0 | 1 | 0 | One bubble counted from depth 17 |
| 22 | 0 | 4 | 0 | |
| 23, 24 | 0 | 0 | 0 | No bubbles |
| Total | 7 | 19 | 0 | |

The results in figure 4.4 and table 4.1 will be discussed further in the next chapter.

### 4.2.2 Bubble Size

The relative size of bubbles is necessary when considering how important missed detections are. Larger bubble size can cause more problems, while smaller might not be a big issue. In this section, the maximum amplitude of the bubbles will be compared to the background signal at the same index, which gives an insight into its size. The amplitude of each missed and falsely detected bubble, and its corresponding background signal, was studied to see why the algorithm made mistakes. By running through every recording in the training set, three Excel files were generated, one containing all detected bubbles, one with false positives and one with missed detections. There were some errors with the missed detections file, so this was generated manually for the training set, but not for the test set. An example of which values are saved to the Excel file is shown in figure 4.7.

| | A | B | C | D | E | F | G |
|---|---|---|---|---|---|---|---|
| 1 | Recording | SingleBubbles | t_datenum | tb | zb | AmpdB | BgsdB |
| 2 | 20190429T115224_IQ_Neo_R3min_P1min_3min_NoIq.mat | 2019:04:29:11:53:18:724 | 737544.495 | 53.7354186 | 12 | 17.7175234 | 8.411873654 |
| 3 | 20190429T115224_IQ_Neo_R3min_P1min_3min_NoIq.mat | 2019:04:29:11:54:04:374 | 737544.496 | 99.3853341 | 12 | 17.2351988 | 7.953273131 |
| 4 | 20190429T115224_IQ_Neo_R3min_P1min_3min_NoIq.mat | 2019:04:29:11:54:32:884 | 737544.496 | 127.895949 | 14 | 18.9028333 | 8.488649826 |
| 5 | 20190429T115224_IQ_Neo_R3min_P1min_3min_NoIq.mat | 2019:04:29:11:54:31:058 | 737544.496 | 126.069952 | 17 | 24.7371087 | 14.89677397 |
| 6 | 20190429T115224_IQ_Neo_R3min_P1min_3min_NoIq.mat | 2019:04:29:11:54:35:401 | 737544.496 | 130.412531 | 17 | 27.6556737 | 17.49683671 |
| 7 | 20190429T115224_IQ_Neo_R3min_P1min_3min_NoIq.mat | 2019:04:29:11:54:26:944 | 737544.496 | 121.95593 | 18 | 26.5294454 | 10.49490547 |
| 8 | 20190429T115224_IQ_Neo_R3min_P1min_3min_NoIq.mat | 2019:04:29:11:54:32:621 | 737544.496 | 127.632986 | 18 | 34.2132332 | 20.54928135 |
| 9 | 20190429T115224_IQ_Neo_R3min_P1min_3min_NoIq.mat | 2019:04:29:11:54:34:784 | 737544.496 | 129.795673 | 18 | 19.2025188 | 8.746586412 |
| 10 | 20190429T115224_IQ_Neo_R3min_P1min_3min_NoIq.mat | 2019:04:29:11:54:30:550 | 737544.496 | 125.561229 | 19 | 34.3151034 | 16.0872224 |
| 11 | 20190429T115224_IQ_Neo_R3min_P1min_3min_NoIq.mat | 2019:04:29:11:54:25:873 | 737544.496 | 120.884417 | 20 | 30.3942592 | 11.35289329 |

**Figure 4.7:** Example of Excel file containing all detected bubbles of the training set

The parameters saved in the Excel files are the name of the recording, *Recording* in column A of figure 4.7, and the time of each bubble in three formats: the one used in EarlyBird which is when the recording was done (both date and time), *SingleBubbles*, the index used in the algorithm to represent this time, *t_datenum*, and the time in seconds from the beginning of the recording, *tb*. The depth of each detected bubble, *zb*, is also saved along with the maximum bubble amplitude, *AmpdB*, and the background signal, *BgsdB*, just before the bubble, both in dB. From these Excel files, histograms can be made to show the distribution of the relative bubble sizes. A histogram showing the maxmimum emboli, or bubble, amplitude (*MaxAmp*) to background amplitue (*Bgs*) ratio (EBR) in the training set is presented in figure 4.8.

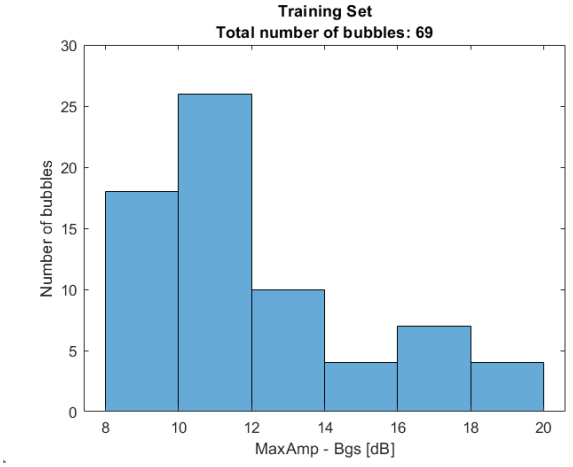


**Figure 4.8:** EBR of all detected bubbles in the training set

From figure 4.8, the maximum amplitude of most bubble signals in the training set are between 10 and 12 dB above the background signal. There are, however, quite a few bubbles between 8 and 10 dB above the background signal as well, and as the threshold is set 9 dB above the background, it seems like the threshold could not be much higher without loosing many bubbles. A lot of the total 69 detected bubbles have a maximum amplitude higher than 12 dB above the background signal, and clearly should be

counted as bubbles if they are not artifacts.

A similar plot of all the missed bubbles of the complete training set is shown in figure 4.9. There were 39 missed detections out of the total 98 manually counted bubbles.

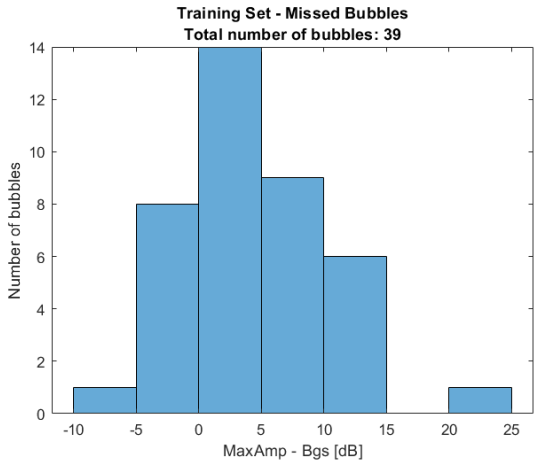


**Figure 4.9:** EBR of all missed bubbles in the training set

There were most missed bubbles with a maximum amplitude between 0 and 5 dB above the background signal. This is quite a lot lower than the threshold of 9dB above the background. There were also 9 bubbles with a maximum amplitude between 0 and 10 dB below the background signal, and 1 bubble with a maximum amplitude between 20 and 25 dB above the background. The bubble with the maximum amplitude more than 20 dB above the background signal had an amplitude of 36 dB in the manual counting. This means that it probably has a large radius and could cause major problems. The background signal was at this point estimated to be 15.1 dB by the algorithm, which is way lower and should make the bubble detectable at more than 9 dB above the background signal. The maximum bubble amplitude was, however, estimated to be 20.7 dB at this index by the algorithm, which is 3.4 dB below the threshold.

The 10 falsely detected bubbles of the training set were also analysed by looking at the ratio between the maximum amplitudes of the detected signals and the background signal at this time in dB. The results are shown in figure 4.10.

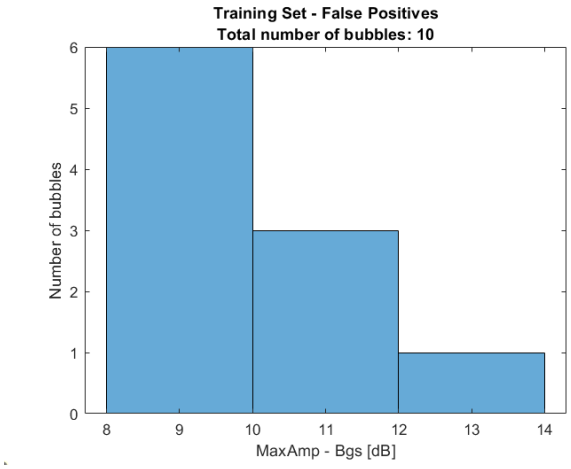


**Figure 4.10:** EBR of all false positives in the training set

All of the false detections naturally had a maximum amplitude more than 9 dB above the background signal as this is the limit to be counted as a bubble by the algorithm. One of the signals even had a maximum amplitude between 12 and 14 dB above the background.

Table 4.2 will only include some of the missed detections of pilot recording 1, comparing the saved amplitudes of the manually counted bubbles to the threshold of the algorithm. All amplitudes in table 4.2 are in dB while time is in seconds.

**Table 4.2:** Amplitude of missed bubbles in pilot recording 1

| **Amplitude of missed manually counted bubbles** | **Threshold** | **Depth** | **Time** |
|---|---|---|---|
| 17 | 24.17 | 11 | 1596 |
| 8 | 17.91 | 12 | 960.1 |
| 18 | 24.57 | 12 | 1048.8 |
| 16 | 22.58 | 17 | 1089.6 |
| 8 | 26.06 | 18 | 1061.6 |
| 4 | 12.30 | 19 | 673.5 |
| 2 | 12.14 | 22 | 731.5 |
| 14 | 15.01 | 22 | 1078.8 |

In some cases, the threshold is a lot higher than the amplitude of the manually counted bubbles. In other cases, like the one in depth 22 at time 1078.8 seconds, the threshold is just over 1 dB above the bubble amplitude. One possible reason is that the amplitude of the signal surrounding the bubble is high due to artifacts, or just have a generally higher intensity. This should in most cases be solved by the median filtering, but a higher intensity signal could still affect the threshold. In some cases, the amplitude of the missed bubble is very low. Two examples are the one in depth 19 at time 673.5 seconds and the one in depth 22 at time 731.5 seconds with an amplitude of only 4 and 2 dB respectively. Their m-mode images are presented in figure 4.11.

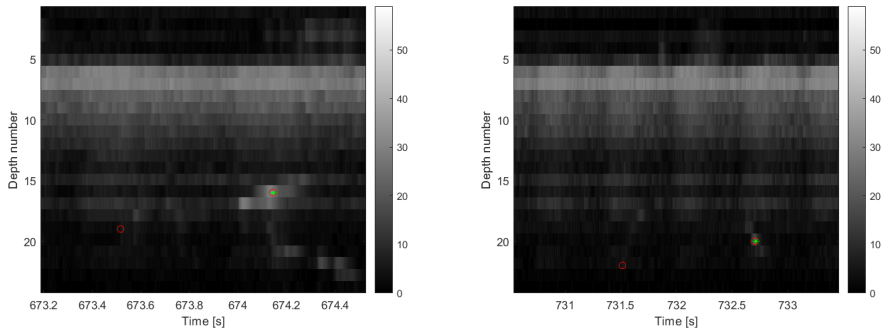


**(a)** Missed bubble in depth 19

**(b)** Missed bubble in depth 22

**Figure 4.11:** M-mode image of two missed bubbles with low intensity

The bubble that was not detected in depth 19 does not immediately seem like a bubble signal by only looking at the m-mode image in figure 4.11a. The background signal generally has a low intensity and the bubble signal is not very clear from this. In the same figure, an example of a correct detection can be seen in depth 16. Figure 4.11b shows another missed bubble signal with low intensity next to a correctly detected bubble in depth 20. The correctly detected bubble stands out from the background signal more than the missed bubble which does not seem to have an intensity much higher than the low background signal. These differences illustrate how high the intensity has to be for the algorithm to detect bubbles.

From the amplitudes in table 4.2, the bubble sizes can be estimated. The bubbles with a small amplitude, like the two previously mentioned in depth 19 and 22, are most likely small and not as critical to detect. They will probably not cause too many issues to the patient. Other bubbles, like the one in depth 11 at time 1596 seconds and in depth 12 at 1048.8 seconds, are probably larger in size and can possibly cause problems like clogging the artery. These bubbles should have been detected, but as can be seen from the table, the threshold was very high in both cases. The m-mode images of the two missed bubbles are shown in figure 4.12.

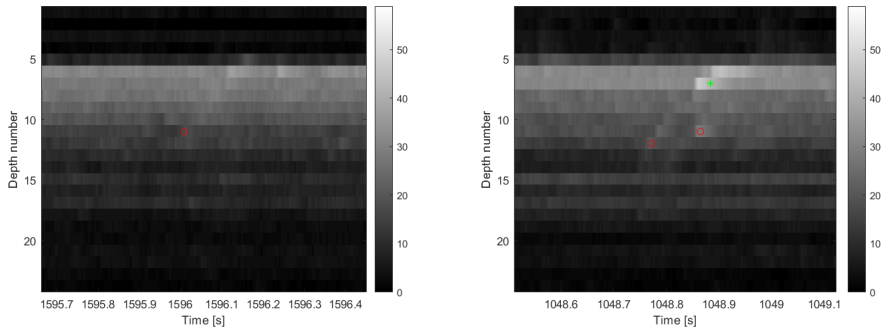


**(a)** Missed bubble in depth 11

**(b)** Missed bubble in depth 12

**Figure 4.12:** M-mode image of two missed bubbles with high intensity

The missed bubble in depth 11, shown in figure 4.12a, seems to be surrounded by a quite high intensity background. This will affect the estimated background signal and make the threshold higher which can result in missed detections as the bubble signal does not stand out a lot from the background signal. The oblique line can be seen by the human eye, but might be more difficult to detect by the algorithm because of the background intensity. This also requires the algorithm to consider multiple depths simultaneously. The same is true for the missed bubble in depth 12 of figure 4.12b. The bubble close by in the same figure has been correctly detected in a different depth. This bubble signal does, however, seem to have an intensity separating it more from the background signal than the one in depth 12.

The training set also consisted of 12 recordings of healthy patients with no bubbles in the blood stream. With the final settings of the algorithm, only 6 bubbles were detected in total as shown in table 4.3, where the counted bubbles in each recording are presented separately. The butterworth LPF was mainly added to avoid too many false positives in these recordings.

**Table 4.3:** Number of counted bubbles in training set recordings with no bubbles

| Recording # without bubbles | 1 | 2 | 3 | 4 | 5 | 6 | 7 | 8 | 9 | 10 | 11 | 12 |
|---|---|---|---|---|---|---|---|---|---|---|---|---|
| Number of detected bubbles | 0 | 0 | 0 | 1 | 0 | 1 | 2 | 1 | 0 | 1 | 0 | 0 |

## 4.3 Test Recordings

The test recordings in this project consisted of recordings from two patients going through heart surgery, and 18 during catheter intervention to fix heart defects. Figure 4.13a shows the ratio of the maximum bubble amplitudes and the background signal in dB for the complete test set.

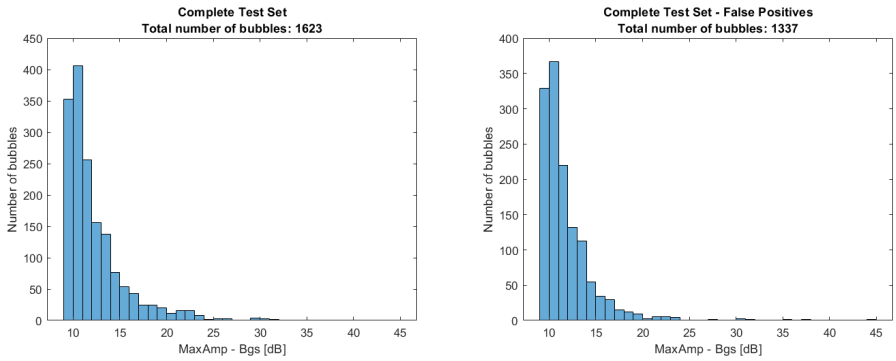


**(a)** All bubbles in the test set

**(b)** All false bubbles in the test set

**Figure 4.13:** EBR of the complete test set

In all recordings of the test set, 1623 bubbles were counted. Just over 400 of these had a maximum amplitude 11 dB above the background signal. Some of the bubbles had an EBR of up to 45 dB but most were below 25 dB. These will be looked into more when considering the two types of patients separately. Of the total number of detected bubbles, most were false positives. 1337 detected bubbles were not detected manually, or were double detections of the same bubble. This will be analyzed later in this chapter.

The total number of manually and automatically detected bubbles, as well as the number of false positives and missed detections are shown for each patient in the test set in table 4.4. The 18 catheter intervention patients are shown on top, with the results of the 2 heart surgery patients below.

**Table 4.4:** Results from test set

| Patient | Manually Counted | Automatically Counted | False Detections | Missed Detections | Correct Detections |
|---|---|---|---|---|---|
| Catheter Intervention Patients | | | | | |
| 1 | - | - | - | - | - |
| 2 | 7 | 19 | 17 | 5 | 2 |
| 3 | 29 | 24 | 8 | 13 | 16 |
| 4 | 13 | 72 | 63 | 4 | 9 |
| 5 | 78 | 400 | 328 | 6 | 72 |
| 6 | - | - | - | - | - |
| 7 | 12 | 13 | 10 | 9 | 3 |
| 8 | 1 | 2 | 1 | 0 | 1 |
| 9 | 9 | 34 | 26 | 1 | 8 |
| 10 | 7 | 220 | 216 | 3 | 4 |
| 11 | 0 | 2 | 2 | 0 | 0 |
| 12 | 0 | 21 | 21 | 0 | 0 |
| 13 | 24 | 102 | 83 | 5 | 19 |
| 14 | 0 | 16 | 16 | 0 | 0 |
| 15 | 148 | 316 | 226 | 58 | 90 |
| 16 | 19 | 19 | 4 | 4 | 15 |
| 17 | 8 | 78 | 74 | 4 | 4 |
| 18 | - | - | - | - | - |
| **Total** | 355 | 1338 | 1095 | 112 | 243 |
| Heart Surgery Patients | | | | | |
| 1 | 21 | 88 | 69 | 2 | 19 |
| 2 | 40 | 197 | 174 | 17 | 23 |
| **Total** | 61 | 285 | 242 | 19 | 42 |

There are large variations in the number of false and missed detections in the test set. Catheter intervention patient 5 has 328 false detections in 60 minutes, patient 10 has 216 in 40 minutes, while patient 15 has 226 false positives in 41 minutes. Other patients, like catheter intervention patient 8, 11 and 16 have only 1, 2 and 4 false detections respectively, detected within 30 to 45 minutes. Some clouds were also manually counted, but are not included in table 4.4. None of them were counted as clouds by the algorithm, but most were detected as single bubbles. In total, 21 clouds were manually detected, where 13 were in catheter patient 5. 2 clouds were counted in catheter patient 9 and 15, while 4 clouds were manually counted in surgery patient 2. The 4 clouds were counted as multiple single bubbles by the algorithm, and caused 13 of the false detections. This is shown in the m-mode image in figure 4.14. As before, the red circles are

manually counted bubbles, green stars are correct automatic detections, while white stars are false positives. The blue circles are manually detected clouds.

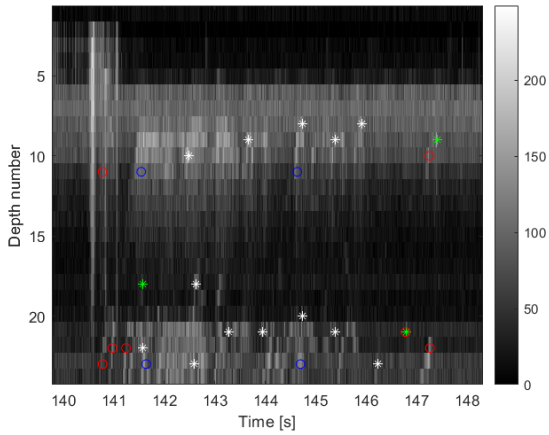


**Figure 4.14:** 4 clouds counted as multiple single bubbles

To get an overview of what types of artefacts or mistakes contribute most to the false positives in the test set, all falsely detected bubbles in the catheter intervention patients with no manually counted bubbles, and catheter intervention patient 2 through 5 were looked into in detail. In catheter patient 2, 3, 4, 5, 11, 12, and 14, a total of 455 fake bubbles were detected in 257 minutes, or 4.3 hours. This means that, on average, 1.77 bubbles were falsely detected every minute in the test set. The false positives were categorized into six different groups as shown in table 4.5.

**Table 4.5:** Number of false positives in each category of a smaller group of recordings

| Type of false detection | Number of detected bubbles |
|---|---|
| Cyclic variations with heart frequency | 385 |
| Movement artifact | 45 |
| Double detection | 15 |
| Cloud | 4 |
| Overlooked bubble | 3 |
| Pulsations of the artery wall | 2 |
| Uncertain bubble | 1 |

There were most false positives due to cyclic variations that follow the heart frequency in the analyzed data set. Roughly 84.6% of the 455 false detections were because of cyclic variations. In these cases, each pulsation of a higher intensity signal

lasts roughly one heart cycle and look like the example shown in figure 4.15 from patient 5 where two false positives are marked. These variations can be seen in almost all recordings in varying degrees. To avoid detecting the signals, the background median filter has to be longer than one heart cycle, roughly 0.25 seconds. In the training set this was not a problem, and the median filter was set equal to roughly 0.246 seconds as a longer window resulted in more false detections in these recordings.

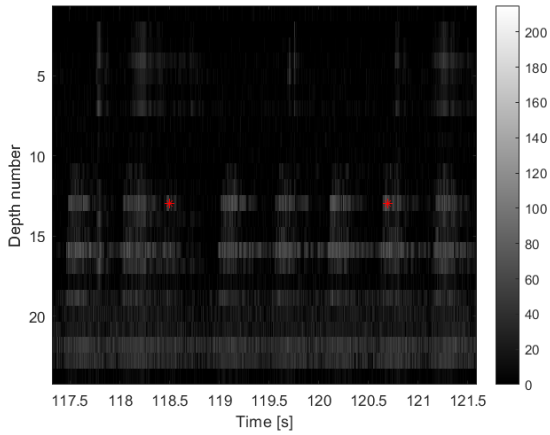


**Figure 4.15:** Cyclic variations with the heart frequency causing false positives

The second most common cause of false detections in the analysis was movement artifacts as previously described. An example is shown in figure 4.16a. Pulsations of the artery wall can also cause the algorithm to detect more bubbles than are actually present. These pulsations are also cyclic, but are shorter in time and depth than the example shown above. Although this did not give that many false positives in the test set, an example from patient 18, which was taken out as described in chapter 3.1.1 but had a lot of false detections due to this, is presented in figure 4.16b.

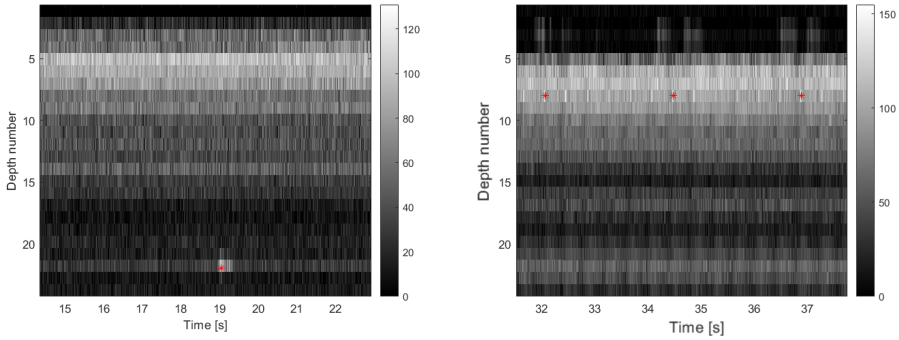


**(a)** Movement artifact

**(b)** Pulsations of the artery wall

**Figure 4.16:** False positives due to two different reasons

15 of the 455 false bubbles in this analysis were caused by double detections of the same bubble signal. These have not been removed by the function *removeDuplicates* in the automatic detection algorithm because they were all too far away from each other, either in time, depht or both. 3 of the bubbles look like bubble signals that have been overlooked and not counted by mistake in the manual detection, while 4 automatic bubble detections were manually counted as clouds. An example of a duplicate detection and a cloud being counted as a bubble, as well as two false detections due to cyclic variations with the heart frequency, is shown in figure 4.17. The cloud is marked by a blue circle in depth 23 around 56.6 seconds.

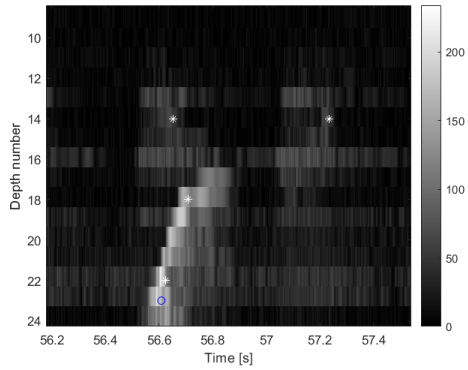


**Figure 4.17:** Detected bubbles in catheter intervention patient 5

The last cause of false positives observed in the analysis was an automatically detected bubble that was manually detected as an uncertain bubble. This is not directly a false positive, and the fact that the algorithm detected it might suggest that it actually is a bubble signal. There is only one example of this in the smaller analysis, which is shown in figure 4.18.

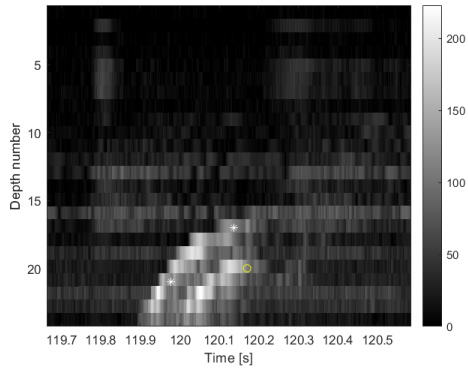


**Figure 4.18:** A bubble marked as *uncertain* in the manual detection that was detected as a bubble by the algorithm

The yellow circle in figure 4.18 in depth 20 at 120.15 seconds marks a bubble that was manually counted as a possible bubble. This was detected twice by the automatic detection algorithm, but neither were marked as correctly detected bubbles.

A similar tendency to the smaller data set that was analysed, can be seen in the remaining recordings. In one recording of catheter intervention patient 15, a lot of false detections were done in the beginning of the signal in multiple depths due to cyclic variations that followed the heart frequency. The m-mode image and the power signal in dB showing the amplitudes are shown in figure 4.19.

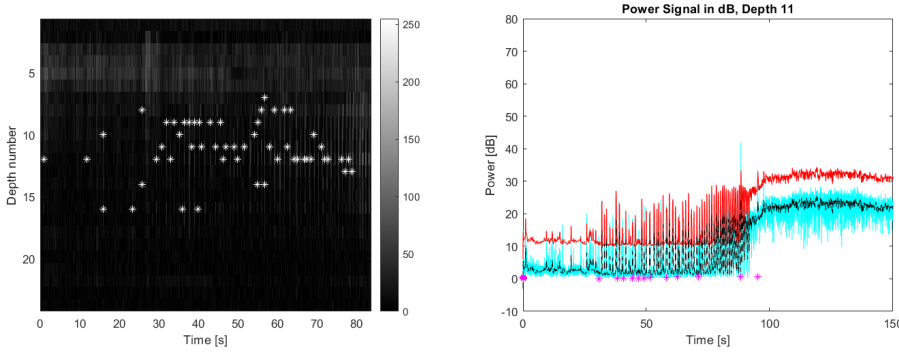


**(a)** M-mode image

**(b)** Power signal in depth 11

**Figure 4.19:** Many false positives in catheter intervention patient 15

The power signal in figure 4.19b shows how the part of the signal before 100 seconds, also shown in depth 11 of the m-mode image of figure 4.19a, has a much lower amplitude than the rest of the signal. All the diastolic velocities, diastiole is the phase of the heart cycle when the heart is filled with blood, are close to 0 in the beginning of the recording, so the cyclic amplitude variations are very large. This resulted in a lot of

false bubbles in depth 7 to 16 at the beginning of the recording. The rest of the power signal mostly stayed around 20 dB.

### 4.3.1 Heart Surgery Patients

In the heart surgery patients, multiple recordings were done before, during, and after the surgery of both patients. The total number of bubbles with their maximum amplitude above the background signal of the individual patients are shown in figure 4.20.

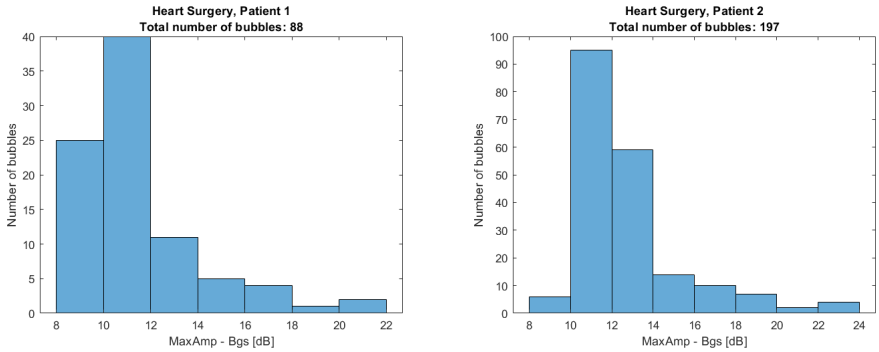


**(a)** Heart surgery patient 1

**(b)** Heart surgery patient 2

**Figure 4.20:** EBR of both heart surgery patients

Although there are more bubbles detected in heart surgery patient 2, the distribution of the maximum amplitude above the background signal is similar in shape. Most detections have a maximum amplitude between 10 and 12 dB above the background signal, while a few have a relative amplitude of up to 24 dB. The combined EBR distribution with the total number of bubbles in both heart surgery patients is shown in figure 4.21.

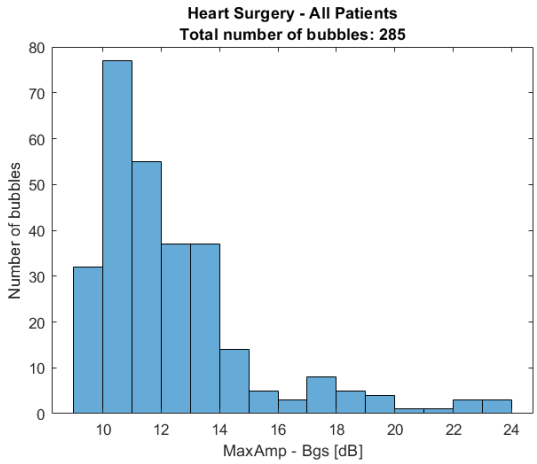


**Figure 4.21:** EBR of both heart surgery patients combined

In the two heart surgery patients, 285 bubbles were detected. Nearly 80 of these had an EBR of 10 dB. There were, however, some bubbles with up to 24 dB amplitudes above the background. Mostly, the EBR stayed between 9 dB and 14 dB, which again shows that the threshold should not be any higher unless a lot of these detections are false positives.

242 of the 285 detected bubbles in the two heart surgery patients were false detections. A histogram showing the distribution of the EBR in these fake bubbles is shown in figure 4.22.

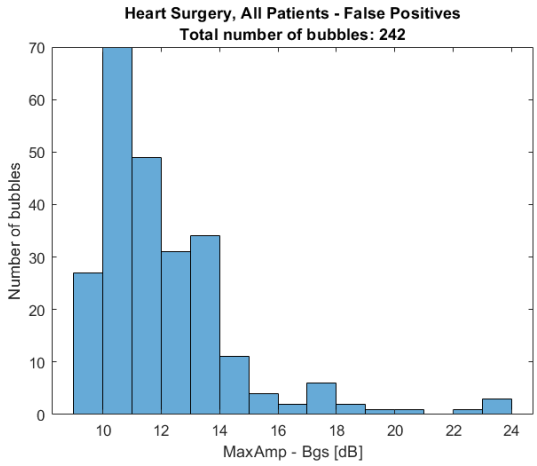


**Figure 4.22:** EBR of false detections of both heart surgery patients

Most of the detected bubbles are false positives, especially the ones with a lower EBR. There are some correct detections with an EBR of 11 dB, but 70 of these nearly 80

bubbles were falsely detected. This indicates that the threshold could have been higher when considering these two patients alone.

### 4.3.2 Catheter Intervention Patients

The recordings of 16 patients going through catheter interventions were analysed, and the total results are shown in figure 4.23.

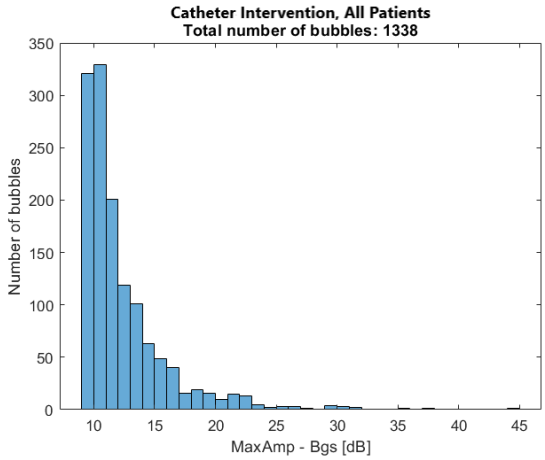


**Figure 4.23:** EBR of all catheter intervention patients

In the catheter intervention patients, 1338 bubbles were counted in total, most of which had a maximum amplitude 10 or 11 dB above the background signal. There were some bubbles with an EBR of up to 45 dB, but most stayed below 25 dB.

There were many fake bubble detections in the catheter intervention patients as shown in figure 4.24. The specific number of false positives for each catheter patient is presented in section 4.3. The EBR of the 1095 false positives have a similar distribution to all detected bubbles, with a peak at 10 to 11 dB. Some detections in the catheter patients had a maximum amplitude up to 45 dB above the background signal, and most of these seem to be false when considering the histogram in figure 4.24.

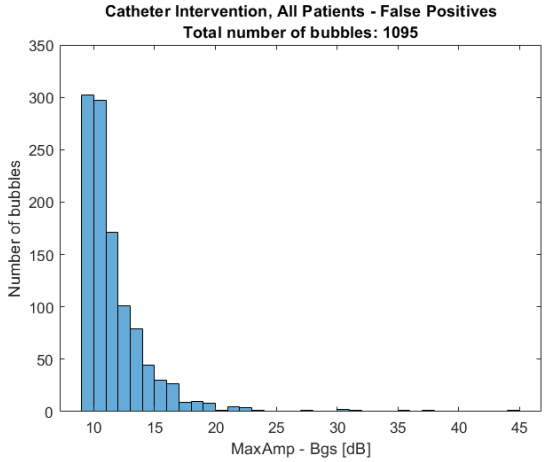


**Figure 4.24:** EBR of false detections of all catheter intervention patients

Chapter 5

# Discussion

## 5.1 Threshold

In the research report *Improved Detection of Microbubble Signals Using Power M-Mode Doppler* [Saqqur et al. [2004]], the threshold was set 3 dB above the maximum background blood flow signal. Using the maximum background signal is a very imprecise way of calculating the threshold, and was not used in this project. Instead, the threshold was found to work best for the training set 9 dB above the background signal found by median filtering. This gives an estimated mean background signal of each point, calculated by the nearest values. Due to this, the threshold is higher than the 3 dB found above the maximum signal in [Saqqur et al. [2004]].

Although different thresholds could have worked better for individual data, 9 dB was the best compromise. This provided as many correct detections without too many false positives in the training set. Even though more correct detections could be done by lowering the threshold or increasing the cutoff frquency, this increased the number of false detections by a lot. An example can be seen in table 3.5 where a cutoff frequency of 30 Hz and a threshold 8 dB above the background signal gave 69 correct detections. The number of false positives in this case was 51, a lot compared to the 10 false positives with the chosen parameters. In comparison, only 10 less missed detections were done.

There are two types of mistakes to consider. Firstly, the number of false detections is important because it could indicate many embolis at times where only cyclic variations are present. This type of mistake does not affect the patient directly, but gives the wrong indication of what medical procedures cause air bubbles. The second type of mistake, missed detections, could be more severe as large bubbles can damage the patient. However, larger bubbles are easier to detect by the algorithm as the EBR, maximum emboli amplitude to background amplitude ratio, is larger, meaning the signal is higher above the threshold than for smaller bubbles.

In conclusion, with 59 correct bubble detections and 10 false positives, a threshold 9 dB above the background signal gave the best results in the training set. Although more correct detections could be made, the number of false detections increased by

so much more that it outweighed the benefits, at least assuming all missed bubbles were of a smaller size. Different thresholds worked best for different recordings, and the variations were very large in some cases, which might explain poor results in some of the recordings.

## 5.2 Training Set

### 5.2.1 Pilot Recording

There are a few reasons why the automatic detection algorithm missed bubbles or counted too many in the pilot recordings. The results are presented in section 4.2.1. The missed bubbles will be discussed first. These are bubbles that were counted manually, the red circles in figure 4.3, but were not detected as bubbles by the algorithm. Some of these bubbles in pilot recording 1 had very low intensity, as seen in table 4.2 and figure 4.11, and the intensity might not be high enough compared to the background signal to be detected. Some other examples, like in figure 4.12, had quite high intensity, but were still not counted. This could be due to a generally higher background signal, or high intensity signals close by which will bring the estimated background signal and threshold up.

There were no false positives in pilot recording 1 with the final settings of the algorithm. There were not that many correctly detected bubbles either due to the threshold being higher than needed for this specific recording. However, with more correct detections using a lower threshold, the more false detections would be made as well. Again, a compromise must be made between the number of correctly detected bubbles and the number of false detections.

The best possible results found for pilot recording 1 were 13 correct detections, 8 false and 13 missed by having no filtering and a threshold 6 dB above the background signal. These are not great results either, and provided up to 140 false detections for the remaining recordings in the training set. There were generally not very good results for pilot recording 1 compared to the other data sets with optimised settings.

Pilot recording 2 only had five manually counted bubbles where three were counted correctly. One false detection was made, and two were missed. Two missed bubbles is not that much, but the maximum amplitude of one of these was 26 dB. The background signal just before the missed bubble signal was, however, also quite high at 21.9 dB, which is why the bubble was not detected. The second bubble had a maximum amplitude of 12 dB with an estimated 13.8 dB background signal just before the bubble. The m-mode image of the two bubbles is shown in figure 4.4b, where they visually do not seem to stand out from the background that much. The recording is quite long, so the fact that only one false detection was made is a good sign. On the other hand, it is difficult to say whether 3 correct detections is good with so few bubbles present.

### 5.2.2 Remaining Training Set

As seen in figure 4.5 and table 3.5, the results using $thresh\_var$ = 9 dB and cutoff $f_c$ = 20 Hz gave OK results, but not the best for all recordings in the training set. Training

recording 1, seen in figure 4.5a, provided quite good results with 34 correct and no false positives. The recording had 49 manually counted bubbles in total which means that 15 were missed. The best results of recording 1 was with no filtering and $thresh\_var = 9.5$ dB. This gave 40 correct detections with no false positives but provided bad results for the recordings without bubbles. The missed recordings, included in figure 4.9 showing the EBR of the complete training set, seemed to be due to their intensity being slightly below the threshold, either because the background signal around the bubble was too high, or because the intensity of the bubble was relatively low. This might be due to the methods used to estimate the background signal. In this project, median filtering with a window size of 0.25 seconds was used, but alternatives should be considered for further development of the algorithm.

Recording 2, seen in figure 4.5b, had three false positives. Most of the manually counted bubbles were detected, only missing 3 in the lower depths (9 to 11). It did, however, falsely detect three bubbles, two of which were in depth 12, earlier in time than the actual bubbles. The background signal seems to vary a lot here, indicating cyclic variations causing false detections. The last false positive was within the group of correctly detected bubbles. By closer inspection, it does look like a bubble signal that might have been missed in the manual counting. The signal is presented in figure 4.6 in the previous chapter. As there are so many bubbles close together in this recording, it seems like the function that compares detected bubbles to manually counted ones might make some mistakes. It is difficult to determine exactly which bubbles are detected where as the time and depth might vary from the manual counting due to the algorithm using the exact maximum intensity of the bubble in the detection. Another thing to consider is that the algorithm might detect the same bubble in multiple depths up to 3 depths apart from the manual detection, but only keeping one of them. If the one furthest apart is kept, it is more difficult to see afterwards which bubble the green star actually detects.

The EBR of most detected bubbles in the complete training set was between 10 and 12 dB as presented in figure 4.8. This means that the maximum amplitude of most bubbles were 10 to 12 dB above the background signal just before the bubble. Some bubbles had an amplitude up to 20 dB above the background, but most had a relative amplitude below 14 dB. The larger a bubble is, the more potential damage it can do to the patient. The large bubbles in the training set are therefore most important to detect, as long as they are actual bubble signals and not noise.

A histogram showing the distribution of the EBR of each missed bubble in the training set is in figure 4.9. There were 39 missed bubbles in total. The deviations in the figure could be explained by the fact that the maximum amplitudes are from the manual detections, while the background signal is estimated with mean filtering of the power signal that sometimes had different amplitudes than the manually registered ones in the same indexes. This seems to be the case for all missed bubbles with a maximum amplitude more than 9 dB above the threshold in figure 4.9. They should, however, be counted. One reason for the differences in the maximum amplitudes could be the low pass filtering of the power signal. This should not change the bubble signal, but with the wrong cutoff frequency, it could happen. This is why the EBR of some bubbles are below zero, or higher than the threshold. One missed bubble had a relative size be-

tween 20 and 25 dB above the background signal according to the histogram. In this case, the manually detected maximum amplitude was a lot higher than the automatically detected amplitude and background signal. The background was estimated at 15.1 dB just before this bubble, with a maximum amplitude of 20.7 dB. This is not more than 9 dB above the background signal which it needs to be for the algorithm to detect it. The manually detected maximum amplitude, however, was 36 dB, which is 20.9 dB above the background. Most of the missed bubbles with a relative size between 0 and 10 dB seemed to have approximately the same estimated amplitude from the manual and automatic detection. These bubbles might not be critical to detect as their sizes are relatively small, assuming the maximum bubble amplitude and background signal are correctly estimated.

The distribution of sizes of the false positives in the total training set is presented in figure 4.10. 10 bubbles were falsely detected in the training set, were 6 of them had a maximum amplitude between 9 (the threshold) and 10 dB above the background signal. These are just large enough to be counted and would not be detected with an increased threshold value. The remaining 4 bubbles had a relative size between 10 and 14 dB, which could imply large bubbles. However, these are from higher intensity signals, either because of variations in the background signal, or from noise.

## 5.3 Test Recordings

The complete test set consisted of 2 heart surgery patients with 57 and 69 recordings each, and 16 catheter intervention patients with a varying number of recordings. 1623 bubbles were detected in total of both groups of patients, with a relative size distribution presented in figure 4.13a. Most of these bubbles had a maximum bubble amplitude to background amplitude ratio (EBR) between 10 and 15 dB with a few exceptions which will be discussed later.

There were generally many false positives in the test set, with up to 328 false detections in one of the catheter intervention patients. In total, 1337 of the 1623 detected bubbles were false positives, roughly 80%. This is a lot, and most were caused by cyclic variations based on the smaller data set were all false detections were looked into in detail. From the results in section 4.3 and table 4.4, the total length of the three patients with most false positives, and the three patients with least false positives were roughly the same. The total length of all recordings of each patient was between 30 and 60 minutes. Although catheter patient 5, which had most false detections at 328, also had the longest total recording time at 60 minutes, patient 10 and 15 also had many false detections with a total recording time of 40 and 41 minutes. This is roughly the same as the total recording time of the patients with fewest false positives. This means that the time of the recordings do not greatly affect the number of false detections. However, if the false positives are due to cyclic variations, a longer recording time will lead to more false positives.

Nearly 70% of the manually counted bubbles in the test set were detected correctly by the automatic detection algorithm. In the catheter intervention patients, a total of 243 bubbles were correctly detected compared to the 355 manually counted bubbles. In the heart surgery patients, 43 bubbles were correctly detected of the 61 manually

counted. All in all, the largest problem in the detection algorithm seems to be the number of false detections. A lot of bubbles are missed as well, but this is connected to the number of false positives as this number increases with more correct detections. Most false detections are due to cyclic variations that follow the heart frequency. This should be avoidable in a future version of the algorithm by considering the length of a heart cycle and when these types of signals show up.

The parameters found to work best for the training set were not optimal for all recordings of the test set. Some patients of the test set had quite good results with few false and missed bubbles, but others had a lot of false and missed detections. The results in table 4.4 show the total number of bubbles of all recordings in each patient. Generally, by rough inspection, it seemed like most false positives in recordings with many fake bubble detections were due to cyclic variations. By lowering the threshold in the algorithm, more correct detections were done in the training set, but more false positives were also detected. This is probably because the cyclic variation differ a lot in intensity and more of them were detected with a lower threshold. If a method is included to detect these variations and avoid counting them as bubbles, the threshold could be set lower, which would provide more correct detections. One way would be to look at the complete signal and check if any higher intensity signals appear frequently with certain intervals, indicating cyclic variations. These indexes and depths could then be saved in a matrix, in a similar way to the artefact detection in the algorithm, to dismiss of any bubbles being detected at these specific times and depths. The current threshold is too high for most recordings of the training set, and probably the test set, but was set this high to avoid false positives. The parameters in the algorithm, like the threshold, are difficult to set to one value fitting all recordings due to large variations in each patient. Some parameters that are now set the same for each patient, should maybe be calculated in a different way based on the signal of each recording.

There were also false detections due to movement artifacts, pulsations of the artery wall, double detections and bubble signals that were overlooked in the manual detection. All of these categories of false positives can possibly be avoided in a new version of the algorithm. Cyclic variations were not particularily a problem in the training set, and was therefore not properly compensated for in the algorithm. There were a lot of double detections in the training set as well, but all of these were within 3 or 4 depths from each other, and no more than 0.5 seconds apart. In the test set, double detections were done despite of the function to remove duplicates because they were further away from each in time, depth or both. Movement artifacts and pulsations of the artery wall were not largely represented in the training set either, and could be better avoided in an improved algorithm.

The rest of the test set results will be discussed in two separate sections. First, the detected bubbles of the 2 heart surgery patients will be considered, before talking about the results of the 16 catheter intervention patients.

### 5.3.1 Heart Surgery Patients

The two patients going through heart surgery that were analysed in this project each had multiple recordings pre, during and post surgery. Patient 1 had 2 recordings pre surgery, 16 during and 39 post surgery, while patient 2 had 4 pre, 16 during and 51 post

surgery.

All detected bubbles in total of the three instances of each patient is presented in figure 4.20. They both follow a similar distribution with most detected bubbles having a maximum amplitude between 10 and 12 dB above the background signal. In patient 1, 88 bubbles were detected, three of which had a maximum amplitude more than 18 dB above the background signal as seen in figure 4.20a. Similarily for patient 2, some bubbles were detected with a maximum amplitude up to 24 dB above the background signal. There were 197 detected bubbles in total for patient 2. All bubbles naturally have an amplitude more than 9 dB above the background as this is the threshold decided for a bubble to be detected. There were 174 false positives in heart surgery patient 2, where 13 were due to 4 clouds being detected as single bubbles, as presented in figure 4.14. This is probably because the signal did not stay above the threshold constantly for a long enough time period. It also seems like the maximum length of a singular bubble, or the minimum length of a cloud, is set too high as this fit the training set best. However, as no clouds were manually counted in the training set, this parameter is likely not ideal.

A histogram showing the combined results of the maximum amplitudes of the 285 detected bubbles is presented in figure 4.21. Nearly 80 bubbles had an amplitude 10 dB above the background signal, while the majority had an EBR between 9 dB and 14 dB. The distribution curve flattens when considering bubbles with an amplitude more than 15 dB above the background signal. The bubbles with a large EBR seem to be large in size and are important to detect as they could lead to the most serious issues for the patient. Bubbles with smaller amplitude and relative size do not cause as dangerous problems and are not as crucial to detect.

The difference in maximum bubble amplitude and background signal of the false positives in the two heart surgery patients is shown in figure 4.22. The plot follows the same distribution as the total bubbles, with a peak of 70 bubbles with an EBR of 11 dB. Some fake bubble detections have a maximum amplitude of up to 24 dB above the background, which usually indicates bubbles with a large radius that can be more harmful. These signals could be from artifacts that were not recognised or shorter high intensity spikes in the signal.

### 5.3.2 Catheter Intervention Patients

There were 16 patients undergoing catheter intervention to fix heart defects in the test set of this project. The total number of detected bubbles in these patients was 1338, where most had an EBR between 10 and 15 dB as seen in figure 4.23. A few had an EBR up to 45dB, which is very large and indicates a large bubble size assuming they are signals from real bubbles and not artifacts, but most stayed below 25 dB.

There were many false positives in the catheter intervention patients as seen in figure 4.24. 1095 of the 1338 automatically detected bubbles were false positives, and some of them had an EBR of up to 45 dB. From this it seems like most detected bubbles with an apparently large bubble radius were false positives. Most of the falsely detected bubbles did, however, have an EBR between 10 and 15 dB, with nearly 350 bubbles 11 dB above the background. 3 of the catheter intervention patients had manually detected clouds, although no clouds were automatically detected. 13 clouds were detected in

patient 5, 2 in patient 9, and 2 in patient 15. These were all detected as single bubbles, where some were disregarded as double detections if they were too close to other bubble detections. The fact that no clouds were automatically detected indicates that the limit between single bubbles and clouds is too high. Currently, a high intensity signal needs to stay above the threshold for more than 40 times the expected bubble length as this gave the best results in the training set. With a lower limit, manually counted single bubbles were detected as clouds. As there were no cloud signals in the training set, this was the only criteria to follow. It also gave correct cloud detections in the shorter recordings that were used in early stages of the development without being part of the training set.

### 5.3.3 Main Cause of False Positives

As presented in table 4.5, one type of artifact caused a lot more false positive detections in the test set than any other. In this analysis, all patients with no manually counted bubbles, and catheter patient 2 through 5 were included as these had a varying number of false detections and hopefully reflects the overall trends of the test set. Of the total 455 false positives in the smaller analysis, 385 were due to cyclic variations with heart frequency. This also caused two false detections in training recording 2, and hugely impact the results of the test set. There clearly needs to be a method of detecting cyclic variations so that they are not counted as bubbles.

The second most prominent type of false detection was due to movement artifacts. This also gave a few false detections in the training set, but was difficult to avoid with the current algorithm going through one depth at a time. 45 of the 455 false positives in the analysis in table 4.5 were due to movement, and a solution to recognise them should be included allthough it is not as critical as the cyclic variations. Double detections is also a problem in the test set although there already is a function to remove duplicates. In these cases, the duplicate detections were further away from each other than the limits set in the duplicate removal function in the algorithm. The limits were set from the results of the training set so that no duplicates were detected in these, but may have to be changed to fit other recordings. This did not, however cause a lot of false positives with only 15 of the 455 in the smaller analysis.

Four more types of false detections were observed in the analysis, but none of them gave a lot of false detections. 4 of the false positives were manually counted as clouds, 3 were due to bubbles possibly overlooked in the manual counting, 2 were because of pulsations of the artery wall, and 1 was manually counted as an uncertain bubble. There is no way to improve the number of false detections due to overlooked or uncertain bubbles in the algorithm, but pulsations of the artery wall was also observed in heart surgery patient 2, and may be something to consider in further development of the algorithm.

## 5.4 Sources of Error

As presented in the discussion on the results from the pilot recording, bubbles might have too low intensity to be counted as bubbles while noise could be seen as a bubble

signal by the algorithm.

Although this does not seem to provide big issues for the algorithm in a recording without too much noise, artifacts from medical instruments can be a big factor. The algorithm might not register all artifacts which can lead to false detections, or the artifacts could increase the overall background intensity, and therefore the threshold, leading to missed detections if the bubble signals are too weak. Movement artefacts is also a large problem. No solution to this was found in the project, but might be possible in further development of the algorithm. The algorithm also did not recognise cyclic variations with the heart frequency, resulting in a lot of false positives in the test set.

It is difficult to know where to separate bubbles and clouds. In this project, the limit was set by trial and error on the recordings in the training set, but an appropriate limit might vary from patient to patient. The signals from different people can be very different, which can lead to the algorithm working very well for some patients, and poorly for others. An example of this is the recordings in the training set which all needed different values of the variable *thresh_var* in order to detect bubbles as correctly as possible.

An important factor is that there were not a lot of recordings or patients in the training set with bubbles. There were enough to see how the algorithm behaves in some different cases, but probably not enough to get a full understanding of how the different parameters should be chosen. An example of this, as previously mentioned, is the fact that the algorithm detects some cyclic variations with the heart frequency as bubbles. Although this phenomena caused two false positives in recording 2 of the training set, it was not represented enough to get a proper basis to detect them. This was a huge problem for some recordings of the test set, and caused most of the false detections.

Chapter 6

# Conclusion

The algorithm was developed and adjusted to fit a training set containing four recordings with bubbles, and 12 without. The most suitable cutoff frequency of an LPF was found to be 20 Hz, which provided the most correct detections without too many false bubbles, especially in the recordings where there were no bubble signals. Multiple threshold values were tested, and the most suitable threshold for each recording varied a lot. A fitting compromise was found to be 9 dB above the background signal estimated by median filtering. In the articles presented in section 1.1.1, the threshold was usually set 3 dB above the maximum background signal, meaning it is higher than the background signal estimated using median filtering. As the values were estimated with quite different methods, it is difficult to compare them directly, and the threshold found in this project is naturally higher than the threshold found to work best in the article by Saqqur [Saqqur et al. [2004]].

The algorithm developed in this project does detect air bubbles passing through the ultrasound beam, and gives an estimated number of bubbles and their placement in time and depth. It is also possible to calculate the relative size of each bubble from the results of the algorithm, and each bubble can be shown visually in an m-mode image of the complete signal in all recorded depths. The detection is, however, not perfect, and the main problem is that a lot of bubbles are falsely detected. 1337 of the 1623 detected bubbles in the complete test set were false bubble detections, mainly due to cyclic variations. In a smaller part of the test set, 385 of the 455 false positives, 84.6%, were due to cyclic variations with the heart frequency.

The algorithm also considers clouds, or curtains, of bubbles, but the detection does not work as wanted. In the training set, the limit between single bubbles and clouds was set so that no manual bubble detections were automatically detected as clouds. This was the only criteria used as there were no manually detected clouds in these recording. There is a counter that counts clouds separate to the single bubbles, but as the limit was set too high, no clouds were detected.

Artifacts are found before any bubble detection is done in the algorithm to avoid falsely detecting them as bubbles. This part of the algorithm seems to work as intended

when considering artifacts due to medical instruments. It does, however, not recognise movement artifacts, cyclic variations or pulsations of the artery wall.

The relative size of each bubble was calculated as EBR, and can be seen from the histograms presented in chapter 4. In general, the algorithm overestimates the number of emboli present in the ultrasound image. Although the algorithm does not provide exact numbers of bubbles in the blood stream, and sometimes gives wrong placements of bubbles, it could be used to get an insight into when bubbles appear during surgery and what procedure was done at the time. It saves a lot of time compared to manually searching for bubbles, which needs to be weighed against the number of missed and false detections of the automatic detection algorithm. The algorithm could possibly be used to recognise bubbles missed in the manual counting if the results from the algorithm and the manual results do not agree. Some examples of this was found in the test set.

## 6.1 Future Work and Improvements

In order to get fewer false detections, the algorithm should neglect high intensity signals appearing in just one depth as this is probably not from a bubble, but could be a movement artifact. Functions to recognise cyclic variations with heart frequency and pulsations of the artery wall should also be included. These types of false detections were not present in a large degree in the training set and were not considerd much in the final algorithm. The cyclic variations differ a lot in intensity, so more were detected with lower thresholds even though this also gave more correct detections. By including functions to take care of false detections due to cyclic variations with the heart frequency, and movement artifacts, the threshold could possibly be lowered, giving more correct detections.

In the test set, some double detections were done because the bubbles stretched further in time or depth than was represented in the training set. In developing the algorithm further, a change in the limits of how far apart the signals can be to be detected as correct bubbles should be considered, as long as they do not affect actual bubbles close by. This does, however, only impact the comparison algorithm and situations were manual detections have been done.

The current limit between singular bubbles and clouds is not fitted for the recordings of the test set. No clouds were automatically detected, while 21 were counted manually. The length a high intensity signal needs to be for cloud detection is too high, and many were counted as single bubbles instead. Recordings with manually counted cloud signals should be included in the training set to get a better basis to distinguish single bubbles from clouds.

The algorithm in this project is not implemented to work in real time, but a future version that detects bubbles consecutively is possible. The algorithm uses roughly half a minute to go through all relevant depths of the m-mode image in the pilot recording of 30 minutes. This is a lot less than the length of the recording which is important if the algorithm is to work in real time.

A possible future solution is to use machine learning to get an algorithm as good as possible with more suited parameter values. At the current time, there are not enough

recordings for this to be plausible. By including more data sets in the training of the algorithm, parameters could also be better suited to the recordings. Some more recordings with clear examples of cyclic variations should be included in the training set so these types of false positives can be avoided.

To get better result, another possible improvement is to have better resolution in the recordings from the NeoDoppler and EarlyBird system. This could potentially improve the detection algorithm, but will lead to other problems such as increased file size and longer run time.

One way to detect some of the missed bubbles is by making the algorithm consider multiple depths at the same time instead of just one like in this project. By determining oblique "lines" in the m-mode image, the algorithm could detect the trail of the bubble signal. This, in turn, would make bubble signals stand out more and avoid double detections along one of these trails.

Further developments of the algorithm should also consider improvements of the filtering as this may have impacted the maximum amplitude of some missed bubbles. However, the best cutoff frequency is very much dependant on the patient and varies a lot from recording to recording. Variations in patients should be considered in a larger degree to get a detection algorithm more suited to each individual case.

# Bibliography

J. J. O'Brien et al. Cerebral emboli during cardiac surgery in children. *American Society of Anesthesiologists*, 87(5):1063–1069, 1997.

M. Saqqur et al. Improved detection of microbubble signals using power m-mode doppler. *Aha Journals, Stroke*, 35:14–17, 2004.

E. B. Ringelstein et al. Consensus on microembolus detection by tcd. *Aha Journals, Stroke*, 29:725–729, 1998.

M. A. Moehring et al. Power m-mode doppler (pmd) for observing cerebral blood flow and tracking emboli. *Ultrasound in Medicine and Biology*, 28(1):49–57, 2002.

U. K. NHS. Embolism, 2020. URL `https://www.nhs.uk/conditions/embolism/`. (accessed: 21.05.2020).

U. S. NIH. Ultrasound, 2016. URL `https://www.nibib.nih.gov/science-education/science-topics/ultrasound`. (accessed: 23.05.2020).

MedlinePlus. Doppler ultrasound, 2019. URL `https://medlineplus.gov/lab-tests/doppler-ultrasound/`. (accessed: 23.05.2020).

ecgwaves.com. Continuous wave doppler (cw doppler), a. URL `https://ecgwaves.com/topic/continuous-wave-doppler-cw-doppler/`. (accessed: 21.07.20).

ecgwaves.com. Pulsed wave doppler, b. URL `https://ecgwaves.com/topic/pulsed-wave-doppler/`. (accessed: 21.07.20).

A. Støylen. Basic doppler ultrasound for technicians. URL `http://folk.ntnu.no/stoylen/strainrate/Basic_Doppler_ultrasound#Clutter_high_pass_filter`. Norwegian University of Science and Technology, Trondheim, Norway.

Lars Hoff. Acoustic characterization of control agents for medical ultrasound imaging. 2000. Norwegian University of Science and Technology, Trondheim, Norway.

M. Minnaert. On musical air-bubbles and the sounds of running water. *Philos. Mag.*, 16:235–248, 1933.

P. Kneppo E. R. Carson and I. Krekule. *Advances in Biomedical Measurement*. Springer Science & Business Media, 2012.

K. Nam et al. Ultrasonic attenuation and backscatter coefficient estimates of rodent-tumor-mimicking structures: Comparison of results among clinical scanners. *HHS Public Access*, 33(4):233–250, 2011.

R. S. C. Cobbold. *Foundations of Biomedical Ultrasound*. Oxford University Press, 2007.

S. A. Evensen. Hematokrit, 2020. URL `https://sml.snl.no/hematokrit`. (accessed: 28.05.2020).

M. T. Lønnebakken, O. Gjesdal, and G. Smith. Ekkokardiografi. URL `https://www.legeforeningen.no/contentassets/1284b55fd78a48999d041c26c3200527/metodebok-2014-7-ekkokardiografi.pdf`. (accessed: 07.06.2020).

A. Murphy, A. Goel, et al. Doppler shift. URL `https://radiopaedia.org/articles/doppler-shift`. (accessed: 30.05.2020).

R. Nave. Arterial ultrasound scan & speed of sound in tissue, 2016. URL `http://hyperphysics.phy-astr.gsu.edu/hbase/Sound/usound2.html`. (accessed: 07.06.2020).

P.N. Devi and R. Asokan. An improved adaptive wavelet shrinkage for ultrasound despeckling. *Sadhana*, 39:971–988, 2014.

J. G. Proakis and D. K. Manolakis. *Digital Signal Processing*. Pearson, 4 edition, 2014.

X. Lai, H. Torp, and K. Kristoffersen. An extended autocorrelation method for estimation of blood velocity. *IEEE Transactions on Ultrasonics, Ferroelectrics, and Frequency Control*, 44(6):1332–1342, 1997.

MathWorks. 1-d median filtering, 2020. URL `https://se.mathworks.com/help/signal/ref/medfilt1.html`. (accessed: 18.07.2020).

S. B. Ritz. Pulmonary stenosis, 2017. URL `https://kidshealth.org/en/parents/pulmonary-stenosis.html`. (accessed: 09.06.2020).

AHA. Aortic stenosis overview, 2020. URL `https://www.heart.org/en/health-topics/heart-valve-problems-and-disease/heart-valve-problems-and-causes/problem-aortic-valve-stenosis`. (accessed: 09.06.2020).

H. Holmström et al. Koarktasjon av aorta (coarctio aortae), 2019. URL https://www.ffhb.no/om-hjertefeil/diagnoser/koarktasjon-av-/. (accessed: 09.06.2020).

Mayo Clinic. Patent ductus arteriosus (pda), 2017a. URL https://www.mayoclinic.org/diseases-conditions/patent-ductus-arteriosus/symptoms-causes/syc-20376145. (accessed: 09.06.2020).

Mayo Clinic. Atrial septal defect (asd), 2019. URL https://www.mayoclinic.org/diseases-conditions/atrial-septal-defect/diagnosis-treatment/drc-20369720. (accessed: 09.06.2020).

Wikipedia. Pericardium, 2020. URL https://en.wikipedia.org/wiki/Pericardium. (accessed: 09.06.2020).

Mayo Clinic. Ventricular septal defect (vsd), 2017b. URL https://www.mayoclinic.org/diseases-conditions/ventricular-septal-defect/symptoms-causes/syc-20353495. (accessed: 09.06.2020).

CCHMC. Transposition of the great arteries, 2019. URL https://www.cincinnatichildrens.org/health/t/transposition. (accessed: 10.06.2020).

C. T. Mai et al. Facts about total anomalous pulmonary venous return or tapvr, 2019. URL https://www.cdc.gov/ncbddd/heartdefects/tapvr.html. (accessed: 10.06.2020).

Mayo Clinic. Tetralogy of fallot, 2017c. URL https://www.mayoclinic.org/diseases-conditions/tetralogy-of-fallot/symptoms-causes/syc-20353477. (accessed: 10.06.2020).

S. D. Vik, H. Torp, T. Follestad, et al. Neodoppler: New ultrasound technology for continuous cerebral circulation monitoring in newborns. *Pediatr Res.*, 2019. Norway.

T. Q. Nguyen. A lumped parameters model for cerebral blood flow in neonates and infants with patent ductus arteriosus. 2019. Norwegian University of Science and Technology, Trondheim, Norway.

A. H. Jarmund. Cerebral hemodynamics in normal neonates during tilt. 2019. Norwegian University of Science and Technology, Trondheim, Norway.

S. Hilgenfeldt et al. Response of bubbles to diagnostic ultrasound: a unifying theoretical approach. 1998. Fachbereich Physik der Universität Marburg, Germany.

K. L. LaRovere et al. Cerebral high-intensity transient signals during pediatric cardiac catheterization: A pilot study using transcranial doppler ultrasonography. *Journal of Neuroimaging*, 27(4):381–387, 2017.

S. Wallace et al. Cerebral microemboli detection and differentiation during transcatheter closure of atrial septal defect in a pediatric population. *Cardiology in the Young*, 25:237–244, 2015.

S. Wallace et al. Cerebral microemboli detection and differentiation during transcatheter closure of patent ductus arteriosus. *Pediatric Cardiology*, 37:1141–1147, 2016.

S. Itoh et al. Microembolic signals measued by transcranial doppler during transcatheter closure of atrial septal defect using the amplatzer septal occluder. *Cardiology in the Young*, 21:182–186, 2011.

R. A. Rodriguez et al. Cerebral blood flow velocities monitored by transcranial doppler during cardiac catheterizations in children. *Catheterization and Cardiocasvular Diagnosis*, 43:282–290, 1998.

Y. Choi et al. A combined power m-mode and single gate transcranial doppler ultrasound microemboli signal criteria for improving emboli detection and reliability. *Journal of Neuroimaging*, 20:359–367, 2010.

J. Molloy and S. M. Hugh. Multigated doppler ultrasound in the detection of emboli in a flow model and embolic signals in patients. *Aha Journals, Stroke*, 27:1548–1552, 1996.

# Appendix

## Automatic Detection Algorithm

```
userVar = struct('N',100,'thresh_var',9,'n_start',7,'n_end',24,'fc',20,'n_artefact',5,'artLim',5,'cloudLength',40,'prevBub',200,'minLength',2,'manual',0);
tic;
N = userVar.N; thresh_var = userVar.thresh_var; n_start = userVar.n_start; n_end = userVar.n_end; fc = userVar.fc; n_artefact = userVar.n_artefact; artLim = userVar.artLim;  cloudLength = userVar.cloudLength; prevBub = userVar.prevBub; minLength = userVar.minLength; manual = userVar.manual;
depthIncr = 0.0016;
%%
if exist('D') == 1
    cmmode = D.Cmmode; %Gets the signal from opened file
else
    cmmode = figh.UserData.Cmmode; %Gets signal straight from Eb software
end
tIncr = cmmode.timeAx(2)-cmmode.timeAx(1); %Finds time increment for the signal
prf = 1/tIncr; %Pulse repitition frequency
if sum(strcmp(fieldnames(cmmode), 'dBStep')) ~= 1 %Checking if cmmode.dBStep exists
  cmmode.dBStep = 1; %If not: set equal to 1
end
%% Plots the signal as m-mode image that is later updated
figure(20); imagesc(cmmode.timeAx,cmmode.depthAx/depthIncr,cmmode.PdB); colormap gray; colorbar; gain=-55; crange = caxis; hold on;
%% Finds power in all depths
pow_dB = cmmode.dBStep*double(cmmode.PdB); %Power in dB for all depths
[depth_iq,~] = size(pow_dB); %Finds number of depths
pow = 10.^(pow_dB/10); %Power for all depths
%% Low Pass Filter
    [b,a]=butter(2,fc/(prf/2)); %Butterworth filter of 2nd order
    pow_dB = filter(b,a,pow_dB,[],2); %Filters pow_dB
%% Checks for artefacts in depths 1:n_artefact
art_detect = zeros(1,length(cmmode.PdB));
for x = 1:n_artefact
    Pow_dB = pow_dB(x,:); %Power in dB for depth n
    Pow = 10.^(Pow_dB/10); %Power in depth n
    bgs_dB = 10*log10(Pow); %Background signal
    thresh = median(bgs_dB) + thresh_var; %Threshold
    for a = 1:length(Pow_dB)
        if (Pow_dB(a) > thresh-1) && (a > artLim) && (a < length(Pow_dB)-artLim)
            art_detect(a) = 1; %This index is registered as an artefact
            art_detect(a-artLim:a+artLim) = 1; %Some artefacts are slightly oblique
        end
    end
end
%% Autocorrelation Estimator to Calculate Doppler shift
t = double(cmmode.timeAx);
velocity = double(cmmode.fi)/128*double(cmmode.vNyquist);
cb = 1570; f0 = 7812500; %f0 from EarlyBird
fd = (2*f0*velocity)/cb; T = abs(10./fd); %fd is the Doppler shift, T the expected length of a potential bubble in each point
```

```
time_bubble_all = {}; time_c_all = {}; bgs_dB_all = {}; thresh_all = {}; maxval_all = {}; Pow_dB_all = {};
%%
for n = n_start:n_end
    Pow_dB = pow_dB(n,:); %Power in dB for depth n
    %% The Automatic Detection Algorithm
    [bubble_bgs,bubble_amp,nbub,time_bubble,time_art,time_c,maxval,thresh,Pow,bgs_dB] = detectBubble(n,minLength,prevBub,cloudLength,N,Pow_dB,T,tIncr,t,art_detect,thresh_var);
    %time_bubble -> time vector for bubbles
    %time_art -> time vector for artefacts
    %time_c -> time vector for clouds
    %maxval -> max value of each bubble, used for plotting
    %thresh -> threshold of this depth (changes every Nth index)
    time_bubble_all{n} = time_bubble; bgs_dB_all{n} = bgs_dB; thresh_all{n} = thresh; bubble_amp_all{n} = bubble_amp;     bubble_bgs_all{n} = bubble_bgs; time_c_all{n} = time_c; nbub_all{n} = nbub; Pow_dB_all{n} = Pow_dB; %Saves the vector of every depth in a struct
end
%% Function for removing duplicates
[time_bubble_all,bubble_amp_all,bubble_bgs_all,nbub_all] = removeDuplicates(bubble_amp_all,bubble_bgs_all,nbub_all,time_bubble_all,n_start,n_end);
toc;
%%
tic;
time_correct_all = {}; time_fake_all = {}; time_miss_all = {}; time_corr_other_depth_all = {}; bubbles = 0; bubbles_correct = 0; bubbles_fake = 0; bubbles_missed = 0; bubbles_manual = 0; clouds = 0;
tb = []; nb = []; bgsb = []; ampb = [];
for n = n_start:n_end
    bgs_dB = bgs_dB_all{n}; thresh = thresh_all{n}; Pow_dB = Pow_dB_all{n};
    time_bubble = time_bubble_all{n}; time_c = time_c_all{n};
    if manual == 1 %Comparison function is run if already manually counted
        [bubbles_manual,bubbles_correct,bubbles_fake,bubbles_missed,time_correct_all,time_fake_all,time_miss_all,time_corr_other_depth_all] = compareBubbles(crange,figh,cmmode,n,time_bubble,time_correct_all,time_fake_all,time_miss_all,time_corr_other_depth_all,bubbles,bubbles_correct,bubbles_fake,bubbles_missed);
        %time_correct -> time vector of correctly counted bubbles
        %time_fake -> time vector of bubbles counted automatically but not manually
        %time_miss -> time vector of bubbles counted manually but not automatically
        %time_corr_other_depth -> time of correctly counted bubbles of other depths
    end
    %% Plotting the power signal and detected bubbles of one chosen depth
    if n == 22
        figure(30);
        plot(t,Pow_dB,'c'); hold on;
        plot(t,thresh,'r',t,bgs_dB,'--k');
        plot(time_bubble,maxval(1:length(time_bubble)),'m*'); %Bubbles counted
        plot(time_c,maxval(1:length(time_c)),'b*'); %Clouds counted
        title('Power Signal in dB, Depth 22');
        xlabel('Time [s]'); ylabel('Power [dB]');
    end
    bubbles = bubbles + nnz(time_bubble); %Total number of bubbles for all depths
    clouds = clouds + nnz(time_c); %Total number of clouds for all depths
    %% In case any vectors are empty:
    if isempty(time_bubble)
```

```
88          time_bubble = inf;
89      end
90      for i = 1:length(time_bubble)
91          if time_bubble(i) == 0
92              time_bubble(i) = inf;
93          end
94      end
95      if manual ~= 1
96          %Plot m-mode image with counted bubbles, this is done in the comparison
                function for already manually counted bubbles
97          figure(20);
98          plot(time_bubble,n,'r*'); caxis(crange);
99          xlabel('Time [s]'); ylabel('Depth number');
100     end
101     tb = [tb nonzeros(time_bubble_all{n}) ']; nb = [nb nonzeros(nbub_all{n}) ']; bgsb
            = [bgsb nonzeros(bubble_bgs_all{n}) ']; ampb = [ampb nonzeros(bubble_amp_all{
            n}) '];
102 end
103 bubbles_fake = bubbles - bubbles_correct; %Total number of falsely detected bubbles
104 bubbles_missed = bubbles_manual - bubbles_correct; %Total number of missed bubbles
105 toc;
106 %% Functions
107 function [bubble_bgs,bubble_amp,nbub,time_bubble,time_art,time_c,maxval,thresh,Pow,
        bgs_dB] = detectBubble(n,minLength,prevBub,cloudLength,N,Pow_dB,T,tIncr,t,
        art_detect,thresh_var)
108     Pow = 10.^(Pow_dB/10); %Power in depth n
109     Filtered = medfilt1(Pow,N); %Median filtering using every Nth point
110     bgs_dB = 10*log10(Filtered); %Background signal in dB
111     thresh = bgs_dB + thresh_var; %Threshold
112     %%
113     a = 1; num_art = 0; c = 0; cloud_count = 0; prev = 0; bubbles = 0;
114     time = zeros(size(t)); time_art = zeros(size(t)); time_c = zeros(size(t));
115     bubble_bgs = []; bubble_amp = []; nbub = [];
116     for i = 1:length(Pow_dB)
117         if i >= a
118         b_length = 0;
119         l_expected = round(T(n,i)/tIncr); %Expected length
120         a = i; %Start index for possible bubble
121             while (Pow_dB(a) > thresh(a)) && (a < length(Pow_dB)) %Finds how long
                    the signal stays above thresh + ending index
122                 b_length = b_length + 1;
123                 a = a + 1;
124             end
125             c = c + 1;
126             [maxval(c),maxind(c)] = max(Pow_dB(i:a)); %index and value of max point
                    from i (start) to a (stops being above threshold)
127             if (i < length(Pow_dB) - maxind(c)) && (art_detect(i + maxind(c)) == 1)
128                 time_art(i + round(maxind(c))) = t(i + round(maxind(c))); %To mark
                        artefacts in figure
129                 num_art = num_art + 1;
130             elseif (i < length(Pow_dB) - maxind(c))
131                 for k = 1:prevBub %To avoid bubbles very close together that are
                        probably the same one
132                     if (i > k) && (time(i - k) ~= 0)
133                         prev = 1;
134                     end
135                 end
```

```
136                 if (b_length > cloudLength*l_expected) && (prev == 0) %Minimum
                        length of cloud
137                     cloud_count = cloud_count + 1;
138                     time_c(i + round(maxind(c))) = t(i + round(maxind(c))); %To mark
                            clouds in figure
139                 elseif (prev == 0) && (l_expected > 0) && (b_length > l_expected/
                        minLength) %Minimum length for bubble
140                     bubbles = bubbles + 1;
141                     bubble_amp(bubbles) = maxval(c);
142                     bubble_bgs(bubbles) = bgs_dB(i);
143                     nbub(bubbles) = n;
144                     time(i + round(maxind(c))) = t(i + round(maxind(c))); %To mark
                            bubbles in figure
145                 end
146             end
147             short = 0; prev = 0;
148         end
149     end
150     if exist('maxval') == 0 %In case there are no bubbles
151         maxval = 0;
152     end
153     time(time==0) = nan; time_bubble = (time(~isnan(time)));
154     time_art(time_art==0) = nan; time_art = time_art(~isnan(time_art));
155     time_c(time_c==0) = nan; time_c = time_c(~isnan(time_c));
156 end
157 %% Function to remove duplicates:
158 function [time_bubble_all,bubble_amp_all,bubble_bgs_all,nbub_all] = removeDuplicates
        (bubble_amp_all,bubble_bgs_all,nbub_all,time_bubble_all,n_start,n_end)
159     for n = n_start:n_end
160         t_bub1 = time_bubble_all{n}; %Times of detected bubbles in depth n
161         for m = n_start:n_end
162             t_bub2 = time_bubble_all{m}; %Times of detected bubbles in depth m
163             for i = 1:length(t_bub1)
164                 for j = 1:length(t_bub2)
165                     diff_t = abs(t_bub1(i)-t_bub2(j)); %Distance in time between the
                            two bubbles
166                     diff_n = abs(n - m); %Distance in depth between the two bubbles
167                     if (diff_t < 0.5) && (diff_n < 4) && (n ~= m) && (
                            time_bubble_all{m}(j) ~= 0) %If close enough in time and
                            depth
168                         time_bubble_all{m}(j) = 0; %Removes duplicate
169                         bubble_amp_all{m}(j) = 0;
170                         bubble_bgs_all{m}(j) = 0;
171                         nbub_all{m}(j) = 0;
172                     end
173                 end
174             end
175         end
176     end
177 end
178 %% Function to compare automatically detected and counted bubbles
179 function [bubbles_manual,bubbles_correct,bubbles_fake,bubbles_missed,
        time_correct_all,time_fake_all,time_miss_all,time_corr_other_depth_all] =
        compareBubbles(crange,figh,cmmode,n,time_bubble,time_correct_all,time_fake_all,
        time_miss_all,time_corr_other_depth_all,bubbles_correct,bubbles_fake,
        bubbles_missed)
180     % All time vectors of bubbles, inclluding correct, false and missed bubbles in
```

```
        previous depths. Updated vectors as output
181     % Get excell data from Eb containing manually counted bubbles
182         ob=guidata(figh);
183         fName=fullfile(ob.datapath,[ob.filename(1:16),'Hits.xlsx']);
184     myTableBub=readtable(fName,'Sheet',1); %Counted bubbles
185         if ~isempty(myTableBub)
186         tb=myTableBub.tb;zb=myTableBub.zb;
187         tbSec=dateNum2sec(figh,tb);
188         AmpdB=myTableBub.AmpdB;
189         for k = 1:length(zb) %Converts the depths of bubbles to right format
190                 [~,zb_fix(k)] = min(abs(cmmode.depthAx-1e-3*zb(k)));
191         end
192     end
193 %{
194     myTableCloud=readtable(fName,'Sheet',2); %Counted clouds
195     if ~isempty(myTableCloud)
196         tc=myTableCloud.tc;zc=myTableCloud.zc;
197         tcSec=dateNum2sec(figh,tc);
198         for o = 1:length(zc) %Converts the depths of bubbles to right format
199             [~,zc_fix(o)] = min(abs(cmmode.depthAx-1e-3*zc(o)));
200         end
201     end
202     myTableU=readtable(fName,'Sheet',3); %Uncertain bubbles
203     if ~isempty(myTableU)
204         tu=myTableU.tu;zu=myTableU.zu;
205         tuSec=dateNum2sec(figh,tu);
206         for h = 1:length(zu) %Converts depths of uncertain bubbles to right format
207             [~,zu_fix(h)] = min(abs(cmmode.depthAx-1e-3*zu(h)));
208         end
209     end
210 %}
211     %%%
212     i_corr = zeros(1,length(tbSec)); i_corr_other_depth = zeros(1,length(tbSec));
            i_miss = zeros(1,length(tbSec));
213     time_corr_other_depth = zeros(1,length(tbSec)); time_fake = zeros(1,length(tbSec
        )); check_detected = zeros(1,length(time_bubble));
214     time_miss = zeros(1,length(tbSec)); time_correct = zeros(1,length(tbSec));
            time_corr_check = zeros(1,length(tbSec));
215     x = 0.1; t1 = 0.5; t2 = 0.3; a = 1; b = 1; l = 1;
216     for i = 1:length(tbSec) %Checking in same depth so that earlier bubbles in other
          depths won't "fill" the spot of a correct spot in the same depth
            diff_d = abs(zb_fix(i)-n);
            for j = 1:length(time_bubble)
                diff_t = abs(tbSec(i)-time_bubble(j));
                if (check_detected(j) ~= 1) && (diff_t < t2) && (diff_d < x) && ((
                    isempty(time_correct)) || (~ismember(tbSec(i),time_correct))) && ((
                    isempty(time_miss)) || (~ismember(tbSec(i),time_miss)))
                    time_correct(a) = tbSec(i);
                    time_correct_all{n}(a) = time_correct(a);
                    i_corr(a) = i;
                    check_detected(j) = 1;
                    a = a + 1;
                end
            end
            if (diff_d == 0) && ((isempty(time_correct)) || (~ismember(tbSec(i),
                time_correct))) && ((isempty(time_miss)) || (~ismember(tbSec(i),
                time_miss))) %To only count bubbles close enough in depth that they
```

```
                should be counted
229             time_miss(b) = tbSec(i);
230             time_miss_all{n}(b) = time_miss(b);
231             i_miss(b) = i;
232             b = b + 1;
233         end
234     end
235     for i = 1:length(tbSec) %Checking for other depths
236         for j = 1:length(time_bubble)
237             diff_t = abs(tbSec(i)-time_bubble(j));
238             diff_d = abs(zb_fix(i)-n);
239             if (check_detected(j) ~= 1) && (diff_t < t1) && ((diff_d == 1) || (
                    diff_d == 2) || (diff_d == 3) || (diff_d == 4)) && ((isempty(
                    time_correct)) || (~ismember(tbSec(i),time_correct))) && ((isempty(
                    time_miss)) || (~ismember(tbSec(i),time_miss)))
240                 time_corr_other_depth(l) = time_bubble(j); %To get exact point for
                        plotting
241                 time_corr_other_depth_all{n}(l) = time_corr_other_depth(l);
242                 i_corr_other_depth(l) = i;
243                 check_detected(j) = 1;
244                 time_corr_check(l) = tbSec(i);
245                 l = l + 1;
246             end
247         end
248     end
249     for l = 1:length(time_bubble)
250         if (check_detected(l) ~= 1)
251             time_fake(l) = time_bubble(l); time_fake_all{n}(l) = time_fake(l);
252         end
253     end
254     bubbles_correct = bubbles_correct + nnz(time_correct) + nnz(
            time_corr_other_depth); %Counts non-zero elements in time vectors
255     %% If any vectors are empty
256         if isempty(time_fake)
257         time_fake = inf; time_fake_all{n} = time_fake;
258     end
259     if isempty(time_correct)
260         time_correct = inf; time_correct_all{n} = time_correct;
261     end
262     if isempty(time_corr_other_depth)
263         time_corr_other_depth = inf; time_corr_other_depth_all{n} =
                time_corr_other_depth;
264     end
265         if isempty(time_bubble)
266         time_bubble = inf;
267     end
268     for i = 1:length(time_bubble)
269     if time_bubble(i) == 0
270             time_bubble(i) = inf;
271         end
272     end
273     for i = 1:length(time_fake)
274         if time_fake(i) == 0
275             time_fake(i) = inf; time_fake_all{n} = time_fake;
276         end
277     end
278     %Plot m-mode image with counted bubbles, updating figure 20
```

```
279     figure(20);
280     plot(tbSec,zb_fix,'ro',tuSec,zu_fix,'yo',time_bubble,n,'g*',time_fake,n,'w*');
            caxis(crange);
281     bubbles_manual = nnz(tbSec); %Number of manually counted bubbles
282     xlabel('Time [s]'); ylabel('Depth number');
283 end
284 %% Function to convert time vectors from EarlyBird to correct format
285 function t=dateNum2sec(figh,tNum)
286     %convert timeaxis tNum from detenum to seconds
287     ob=guidata(figh);
288     t=(tNum-datenum(ob.acq_p.date_time))*60*60*24;
289 end
```

# Blood and Bubble Simulation - Code by Hans Torp

```
% Respons singlescatters and blood
% 2020.03.15 Hans Torp
% 2020.03.26 version 2
%%
close all; clear; clc;
%addpath('/Users/htorp/Dropbox/Hans/Matlab/Field_II_ver_3_22_mac');
field_init;
%% setup transducer
c=1540;%lydhastighet
f0=7.8e6;%frekvens
fs=300e6;
att=0.5;%dB/cm/MHz
lambda=c/f0;
elem_size=0.1e-3;
Rxd=5e-3;
set_sampling(fs);
if exist('Th'),xdc_free(Th);clear Th; end;
Th = xdc_piston (Rxd,elem_size);

% Tx pulse
Tp=10/f0;
impulse_response=sin(2*pi*f0*(0:1/fs:2/f0));
impulse_response=impulse_response.*hanning(max(size(impulse_response)))';
xdc_impulse(Th, impulse_response);
excitation=sin(2*pi*f0*(0:1/fs:Tp));
xdc_excitation (Th, excitation);
Nz=40;Nx=50;Ny=40;
xmax=8e-3;
ymax=6e-3;
zmax=40e-3;
xaxis=linspace(-xmax,xmax,Nx);
yaxis=linspace(-ymax,ymax,Ny);
zaxis=linspace(1e-3,zmax,Nz);
attCorr=10.^(-zaxis*100*att/10*f0/1e6);

%% x profile
depth=20e-3;
%points=[zeros(Nz,2),zaxis'];
points=[xaxis',zeros(Nx,1),zeros(Nx,1)+depth];

[rfZ,start_time]=calc_hhp(Th,Th,points);
xprofile=mean(rfZ.^2);
xprofile=xprofile/max(xprofile);
figure(1);
plot(xaxis,10*log10(xprofile));

%% Doppler signal from single buble
prf=9.76e3/4;
v=-0.03;
fi=60/180*pi;
Nt=800;%number of timepoints 2*Nt+1
T=Nt/prf;
t=(-Nt:Nt)/prf;t=t';
y0=4e-3;x0=0;z0=20e-3;%centerpoint of trajectory
points=[x0-v*sin(fi)*t,y0+0*t,z0-v*cos(fi)*t];%positive velocity towards transducer(
```

```
    negative z direction
[rfx,start_time]=calc_hhp(Th,Th,points);%Pulse echo response
[Ntf,Nts]=size(rfx);
tf=start_time+(0:Ntf-1)/fs;
zax1=c/2*tf;
Qdec=10;
rfDec=resample(rfx,1,Qdec);%decimate to fs=30 MHz
rfDec=rfDec/max(rfDec(:));
NtD=size(rfDec,1);
iq1=hilbert(rfDec);

figure(2);
nt=round(NtD/2);
subplot(2,1,1);plot(t,real(iq1(nt,:)),t,imag(iq1(nt,:)));

mmode=20*log10(abs(iq1));
subplot(2,1,2);imagesc(t,zax1,mmode);colormap gray;colorbar;
caxis([-40,0]);

%% Blood and bubble scatterers
Trec=2;% recording time
Dvessel=3e-3;%diameter blood vessel
dz=c/2/fs*Qdec;%depth increment in zdirection
Nr=round(Dvessel/sin(fi)/dz);%N samples in z-direction
dt=1/prf;
NTrec=round(Trec/dt);
sScatBlood=randn(Nr,NTrec);% blood scatterers in  blood vessel
% Bubble scatterers
sScatBubles=0*sScatBlood; %%HERFRA: KAN LEGGE INN ENKELTBOBLER OG SKYER
nzBub=round(Nr/2);%bubble in center of blood vessel
tBub=Trec/2;ntBub=round(1+tBub/dt);%bubble at time tBub
sScatBubles(nzBub,ntBub)=500;%1000;%one buble in position (nzBub,ntBub) in array
    sScatBubles
tBub=Trec/2+0.3;ntBub=round(1+tBub/dt);%bubble at time tBub %tBub=Trec/2+0.03;
sScatBubles(nzBub,ntBub)=500;%one more buble in position (nzBub,ntBub) in array
    sScatBubles
tBub=Trec/2+0.4;ntBub=round(1+tBub/dt);%bubble at time tBub %tBub=Trec/2+0.03;
sScatBubles(nzBub,ntBub)=500;%one more buble
tBub=Trec/2+0.5;ntBub=round(1+tBub/dt);%bubble at time tBub %tBub=Trec/2+0.03;
sScatBubles(nzBub,ntBub)=500;%one more buble
% Add cloud of bubles
tCloud=0.1;ntCloud=round(1+tCloud/dt);%start-time cloud
Tcloud=0.2;Ncloud=round(Tcloud/dt);% duration cloud
sScatBubles(:,ntCloud+(1:Ncloud))=10*randn(Nr,Ncloud);%lot of randomly distributed
    bubbles

sScat=sScatBlood+sScatBubles;
%% convolution to get signal from blood + bubbles (this will take some time to
    calculate...)
tic
s= conv2(rfDec,sScat);
iq=hilbert(s);
toc
%% Display total signal
Nz=size(iq,1);
zAx= z0 + (-Nz/2:Nz/2)*dz;
iqNoise=0.2*Nr*(randn(size(iq))+i*randn(size(iq)));%thermal noise
```

```
108 iqTot=iq+iqNoise;%iq signal including thermal noise
109 figure(3);
110 trec=(1:size(iq,2))*dt;
111 subplot(2,1,1);
112 nt=round(size(iq,1)/2);
113 plot(trec,real(iqTot(nt,:)),trec,imag(iqTot(nt,:)));
114 subplot(2,1,2);
115 imagesc(trec,zAx,20*log10(abs(iqTot)));colormap gray;colorbar
116 gain=-60;
117 caxis([-40,0]-gain);
```

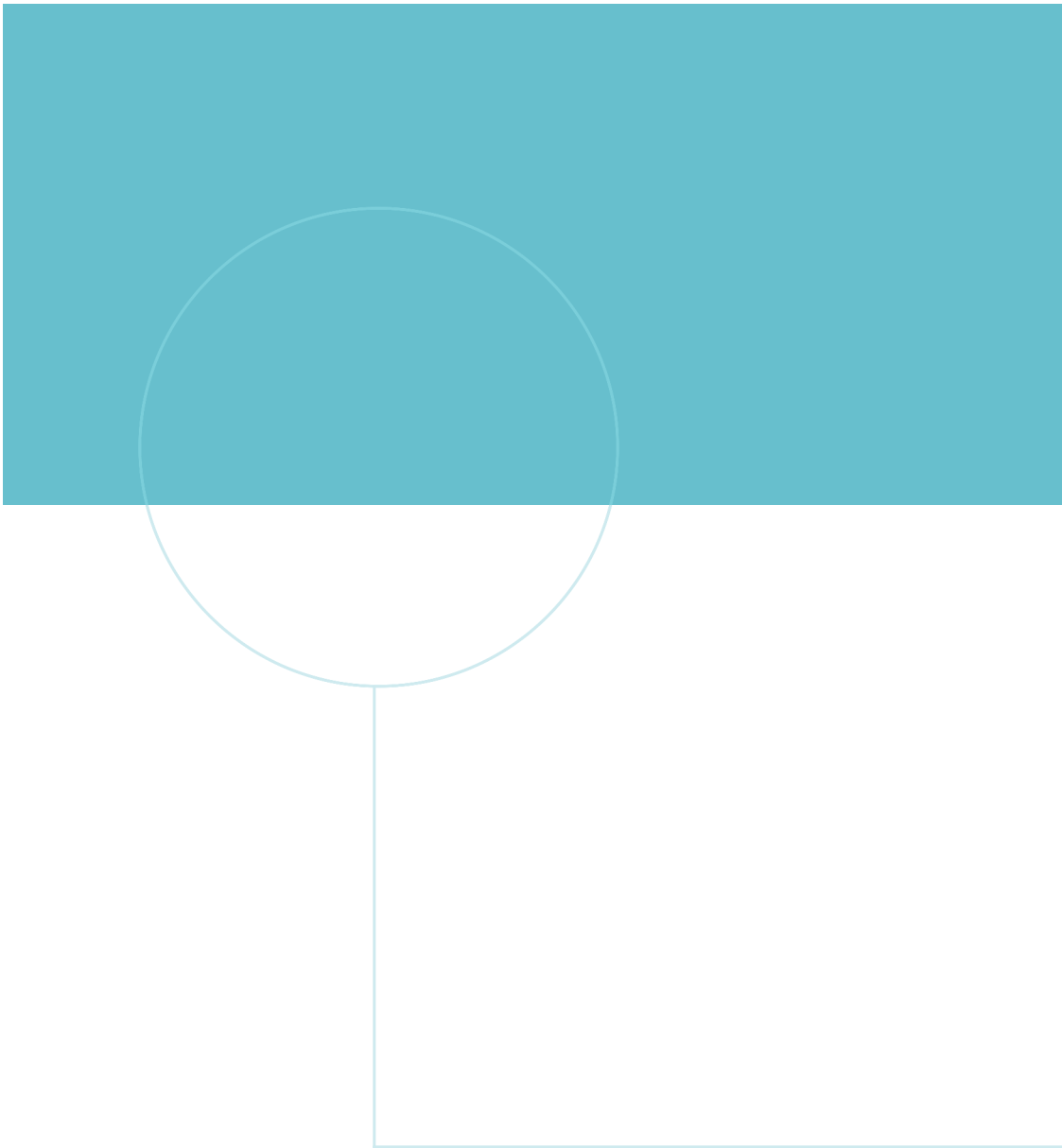

NTNU

Norwegian University of
Science and Technology